Corrosion Inhibition of Copper by Thioureas and N, O, S-Ligating Ring Compounds

Sontaya Manaboot

A Thesis Submitted in Partial Fulfillment of the Requirements for the Degree of Master of Science in Chemistry

Prince of Songkla University

2017

Thesis Title	Corrosion Inhibition of Copper by Thioureas and N, O, S Ligating Ring Compounds
Author	Mr. Sontaya Manaboot
Major Program	Chemistry

Major Advisor

……
(Asst. Prof. Dr. Pipat Chooto)

Co-advisor

……
(Dr. Weena Aemaeg Tapachai)

……
(Dr. Supunnee Duangthong)

Examining Committee:

…….Chairperson
(Asst. Prof. Dr. Charuwan Khamkaew)

……..……Committee
(Asst. Prof. Dr. Pipat Chooto)

……..……Committee
(Dr. Weena Aemaeg Tapachai)

……..……Committee
(Dr. Supunnee Duangthong)

……..……Committee
(Dr. Puchong Wararatananurak)

The Graduate School, Prince of Songkla University, has approved this thesis as partial fulfillment of the requirements for the Master of Science Degree in Chemistry

……
(Assoc. Prof. Dr. Teerapol Srichana)
Dean of Graduate School

This is to certify that the work here submitted is the result of the candidate's own investigations. Due acknowledgement has been made of any assistance received.

..... Signature
(Asst. Prof. Dr. Pipat Chooto)
Major Advisor

..... Signature
(Mr. Sontaya Manaboot)
Candidate

I hereby certify that this work has not been accepted in substance for any other degree, and is not being currently submitted in candidature for any degree.

..... Signature

(Mr. Sontaya Manaboot)

Candidate

ชื่อวิทยานิพนธ์ การป้องกันการกัดกร่อนของโลหะทองแดงด้วยสารประกอบไทโอยูเรียและลิแกนด์ทีมีอะตอมไนโตรเจนออกซิเจนและซัลเฟอร์เป็นองค์ประกอบ

ผู้เขียน นายสนธยา มานะบุตร

สาขาวิชา เคมี

ปีการศึกษา 2559

บทคัดย่อ

สารประกอบไทโอยูเรียและสารในกลุ่มลิแกนด์ที่มีอะตอมไนโตรเจน ออกซิเจน และซัลเฟอร์เป็นองค์ประกอบถูกศึกษาพฤติกรรมการยับยั้งกันการกัดกร่อนแก่ทองแดงในอะซีโตไนไตรล์ จากการศึกษาสารประกอบควิโนนได้แก่ xanthone, xanthene, thioxanthone, acridone และ 1,4-naphthoquinone พบว่า acridone เป็นตัวยับยั้งที่ดีที่สุดโดยประสิทธิภาพในการยับยั้งการกัดกร่อนเท่ากับ 98.98% ขณะที่สารประกอบ 1,4-naphthoquinone มีประสิทธิภาพในการยับยั้งกันการกัดกร่อนต่ำสุดเนื่องจากปฏิสัมพันธ์ที่อ่อนระหว่างหมู่คาร์บอนิลและทองแดง เนื่องจากซัลเฟอร์สามารถเกิดพันธะที่แข็งแรงกับทองแดงทำให้สารในกลุ่มไทโอยูเรียมีพฤติกรรมการยับยั้งการกัดกร่อนสูงกว่าสารในกลุ่มควิโนน สำหรับพฤติกรรมการยับยั้งการกัดกร่อนของสารประกอบในกลุ่มไทโอยูเรีย ได้แก่ thiourea, diphenylthiourea, phenylthiourea และ ethylenethiourea พบว่า ethylene thiourea แสดงประสิทธิภาพในการยับยั้งการกัดกร่อนสูงสุดที่ 99.48% และ diphenylthiourea มีประสิทธิภาพในการยับยั้งการกัดกร่อนต่ำสุดเนื่องจากความเกะกะของหมู่ฟีนีลในโครงสร้างและประสิทธิภาพในการยับยั้งการกัดกร่อนของไทโอยูเรียลดลงเมื่อเติมเฮไลด์ไอออนสามชนิด ได้แก่ คลอไรด์ โบรไมด์ และ ไอโอไดด์ เนื่องจากไอออนดังกล่าวสามารถเกิดสารประกอบเชิงซ้อนกับทองแดงได้ดีกว่าสารประกอบไทโอยูเรีย โดยไอโอไดด์สามารถเข้าจับกับทองแดงได้ดีที่สุดจากการศึกษาด้วย X-ray crystallography และ Cyclic voltammetry

ประสิทธิภาพในการยับยั้งการกัดกร่อนของ dimedone ทีมีต่อโลหะทองแดงในอะซิโตไนไตรล์ถูกศึกษาด้วยเทคนิค potentiodynamic polarization และ electrochemical impedance spectroscopy (EIS) พบว่า dimedone มีประสิทธิภาพในการยับยั้งการกัดกร่อนแก่ทองแดงสูงสุด 93.68% ที่ความเข้มข้น 3.0 mM ชี้ให้เห็นว่าโมเลกุลของ dimedone ดูดซับบนผิวหน้าทองแดงแล้วเกิดเป็นฟิล์มเคลือบป้องกันการเกิดปฏิกิริยาที่ผิวหน้าทองแดง

จากการศึกษาด้วย Cyclic voltammetry พบว่าพีคออกซิเดชันของทองแดงลดลงซึ่งเป็นผลมาจากการเกิดสารประกอบเชิงซ้อนกับ dimedone และจากกราฟ polarization ชี้ให้เห็นว่า dimedone เป็นตัวยับยั้งแบบผสมซึ่งการดูดซับบนผิวหน้าทองแดงเป็นไปตามไอโซเทอมของ Langmuir โดยกลไกลการดูดซับเป็นการดูดซับทางกายภาพเนื่องจากพลังงานอิสระของการดูดซับ (ΔG^{o}_{ads}) ที่คำนวณจากผลที่ได้จากเทคนิค polarization และ impedance มีความสอดคล้องกันคือ -8.43 และ -8.17 kJmol-1 ตามลำดับ ผลจาก Fourier transform infrared spectroscopy (FTIR) ยืนยันการเกิดปฏิสัมพันธ์ระหว่างทองแดงกับออกซิเจนในโครงสร้างของ dimedone โดยสัดส่วนโมลของสารประกอบเชิงซ้อน copper-dimedone ทดสอบด้วยวิธี mole ratio พบว่ามีสัดส่วนเท่ากับ 1:2 และจากภาพถ่ายผิวหน้าทองแดงด้วยกล้องจุลทรรศน์อิเล็ก-ตรอนแบบส่องกราด (SEM) หลังแช่แผ่นทองแดงในสารละลาย dimedone พบว่ามีชั้นฟิล์มเคลือบบนผิวหน้าทองแดง ผลจากการคำนวณทางเคมีควอนตั้มพบว่าแถบช่องว่างพลังงาน (ΔE) ระหว่างออร์บิทัลของโมเลกุลที่มีพลังงานสูงที่สุดที่มีอิเลคตรอนบรรจุอยู่ (E_{HOMO}) กับออร์บิทัลของโมเลกุลที่มีพลังงานต่ำที่สุดที่ไม่มีอิเลคตรอนบรรจุอยู่ (E_{LUMO}) มีค่าน้อยชี้ให้เห็นว่าเห็นได้ว่าโมเลกุลของ dimedone สามารถดูดซับบนผิวหน้าทองแดงได้ดีมีผลให้ประสิทธิภาพในการยับยั้งการกัดกร่อนเพิ่มขึ้น

Thesis Title Corrosion Inhibition of Copper by Thioureas and N, O, S-Ligating Ring Compounds

Author Mr. Sontaya Manaboot

Major Program Chemistry

Academic Year 2016

ABSTRACT

Certain N, O, S-ligating ring compounds and thioureas were investigated to understand their role of inhibiting copper corrosion in acetonitrile. For 5 quinones under study including xanthone, xanthene, thioxanthone, acridone and 1,4-naphthoquinone, acridone is the best inhibitor with the corrosion inhibition of 98.98% whereas 1,4-naphthoquinone exhibits the lowest inhibition, due to weak interaction between carbonyl group and copper. With the presence of sulphur to form stronger bond with copper, thioureas have better inhibiting behavior than quinones. For 4 thioureas namely thiourea, diphenylthiourea, phenylthiourea, and ethylenethiourea; ethylene thiourea derivatives shows the best inhibition with the corrosion inhibition of 99.48% and diphenylthiourea the lowest due to steric effect from phenyl group. When halide ions are present, the efficiency of thioureas in inhibition decreases due to more preferable copper complexation to halides, with the strongest copper-halide bond formation by the free iodide ion, consistent with the results from X-ray crystallography and Cyclic voltammetry.

The inhibition ability of dimedone for copper in acetonitrile at 25 ^{o}C was investigated by potentiodynamic polarization and electrochemical impedance spectroscopy (EIS). Corrosion resistance was found to be increased with inhibitor concentration up to 93.68% inhibition efficiency at 3.00 mM, indicating that dimedone molecules can cumulatively adsorb on the copper surface and finally form a protective film on copper-solution interface. This is also supported by the decreasing of copper oxidation in cyclic voltammogram. Polarization curves revealed that dimedone is of mixed type inhibitor. The adsorption of dimedone on copper surface obeys the Langmuir isotherm and the adsorption mechanism is of physisorption type. The standard energy of adsorption (ΔG^{o}_{ads}) values were found in good agreement for

both polarization and impedance to be -8.43 and -8.17 $kJmol^{-1}$ respectively. Fourier Transform Infrared spectroscopy (FT-IR) confirmed the interaction of copper with oxygen on dimedone. The mole ratio method suggested that the complexation ratio of copper-dimedone is 1:2. Scanning electron microscopy (SEM) of copper surface after immersion in dimedone solution indicates the presence of a protective layer on the electrode surface. The frontier molecular orbital energy E_{HOMO} (highest occupied molecular orbital), E_{LUMO} (lowest unoccupied molecular orbital), and the Mulliken charge distribution obtained from Quantum chemical calculations revealed that the small value of energy gap (ΔE) for dimedone reflects strong adsorption of the molecules on copper surface. The enhanced corrosion inhibition is possibly due to the compact film structure blocking the electron transfer from the solution to copper surface.

ACKNOWLEDGEMENT

The completion of this thesis is fulfilled with the help of certain people whom I am so grateful to.

Firstly I deeply express my sincere thanks to my advisor Assist. Prof. Dr. Pipat Chooto, Dr. Supannee Duangthong, Dr. Weena Aemaeg Tapachai and Dr. Puchong Wararatananurak for their valuable advice and suggestions throughout the course of this work,

Next I would like to thank:

The examination committee members of this thesis for their valuable time,

The Graduate school for financial support and Department of Chemistry, Prince of Songkla University for chemicals and equipment,

My parents and my brothers for their loves and attention all through my life,

Finally, I would like to express my special appreciation go to all my friends in Analytical Chemistry as well as in other who are always of great help and support.

Sontaya Manaboot

CONTENTS

CONTENTS (CONTINUED)

CONTENTS (CONTINUED)

LIST OF TABLES

LIST OF FIGURES

LIST OF FIGURES (CONTINUED)

LIST OF FIGURES (CONTINUED)

LIST OF ABBREVIATIONS AND SYMBOLS

A	=	Absorbance
ω	=	Angular frequency
b_a	=	Anodic Tafel coefficient
β_a	=	Anodic Tafel slope
j_{anode}	=	Anodic current density
E_p^a	=	Anodic peak potential
i_p^a	=	Anodic peak current
K_{ads}	=	Adsorption equilibrium constant
Asp	=	Aspartic acid
Asn	=	Asparagine
Ala	=	Alanine
Arg	=	Arginine
BTA	=	Benzotriazole
E_{corr}	=	Corrosion potential
j_{corr}	=	Corrosion current density
β_c	=	Cathodic Tafel slope
b_c	=	Cathodic Tafel coefficient
$J_{cathodie}$	=	Cathodice current desity
R_{ct}	=	Charge transfer resistance
CV	=	Cyclic Voltammetry
E_p^c	=	Cathodic peak potential
i_p^c	=	Cathodic peak current
dptu	=	Diphenyl Thiourea
^oC	=	Degree Celsius
C_{dl}	=	Double layer capacitance
θ	=	Degree surface covered
D	=	Dipole moment
EIS	=	Electrochemical impedance spectroscopy
E_{eq}	=	Equilibrium potential
ε	=	Epsilon

LIST OF ABBREVIATIONS AND SYMBOLS (CONTINUED)

etu	=	Ethylene Thiourea
EFM	=	Electrochemical frequency modulation
EC	=	Equivalent circuit
F	=	Faraday constant
FTIR	=	Fourier transform infrared spectrometry
Glu	=	Glutamic acid
Gln	=	Glutamine
g mol^{-1}	=	Gram per mole
g cm^{-3}	=	Gramper per cubic
E_{HOMO}	=	Highest occupied molecular orbital
His	=	Histidine
J mol^{-1} K^{-1}	=	Joules per mole kelvin
kJ mol^{-1}	=	Kilojoule per mole
j_L	=	Limiting current
E_{LUMO}	=	Lowest unoccupied molecular orbitals
Lys	=	Lysine
Met	=	Methionine
mM	=	Millimolar
n	=	Number of participating electrons
V-pph-V	=	N, N'-*p*-phenylen-*bis* (3-methoxy-salicylidenimine)
V-oph-V	=	N,N'-*o*-phenylen-*bis*(3-methoxy salicylidenimine
V-his	=	N'-histidine-3-methoxy-salicylidenimine
$\Omega.cm^2$	=	Ohm per centimeter square
η	=	Overpotential
OCP	=	Open circuit potential
Pm	=	Picometre
E_{pp}	=	Passivation potential
E	=	Potential

LIST OF ABBREVIATIONS AND SYMBOLS (CONTINUED)

b	=	Path length of the sample cell
π	=	Pi
Pro	=	Proline
Phe	=	Phenylalanine
PTh-AQSA	=	Polythiophene-anthraquinone Sulphonic acid
ptu	=	Phenyl Thiourea
R_s	=	Solution resistance
E^O	=	Standard potential
SEM	=	Scanning electron microscopy
ΔG^o_{ads}	=	Standard Gibbs free energy of adsorption
b	=	Tafel slope
T	=	Temperature
$TBAPF_6$	=	Tetrabutylammonium-hexafluorophosphase
Tyr	=	Tyrosine
Try	=	Tryptopane
TU	=	Thiourea
UV	=	Ultraviolet
R	=	Universal gas constant (8.314 $mol^{-1}K^{-1}$)
V/decade	=	Vole per decade
BTA-MeOH	=	1-H-benzotriazole-methanol
BQ	=	1,4-Benzoquinone
NQ	=	1,2-Naphthoquinone
PU	=	1,2,4-Trihydroxy-anthraquinone
AAQ	=	1-Amino-4-hydroxy-anthraquinone
AAQs	=	1-aminoanthraquinone
AL	=	1,2-Dyhydroxy-anthraquinone
MBQ	=	2-Methylbenzo-quinone
MTP	=	2-(5-mercapto1,3,4thiadiazole-2-yl)-phenol

LIST OF ABBREVIATIONS AND SYMBOLS (CONTINUED)

AMTa	=	3-amino-5-mercapto1,2,4-triazole film
ATT	=	4-amino-4H-1,2,4-triazole-3thiol
AMTT	=	4-amino-5-methy l-4H-1,2,4-triazole-3thiol
AETT	=	4-amino-5-ethyl-4H-1,2,4-triazole-3thiol
PTT	=	5-phenyl-1,3,4-thiadiazole-2-thiol

CHAPTER 1

INTRODUCTION

1.1 Introduction

Copper has long been used in a number of areas, especially as a structural component due to its advantageous properties especially in marine systems (Liao et al., 2011; Zhang et al., 2011). However, the presence of Cl^- makes it vulnerable to corrosion and makes corrosion inhibition economically important. There are a variety of ways to inhibit copper corrosion; the most promising is the use of certain organic compounds, via the mechanism of adsorption as well as complex formation (Zhao and Cui, 2011). There are a number of researches involving the use of N-containing compounds especially triazoles for corrosion inhibition (Sharif et al., 2007; Pan et al., 2013; Sudheer and Quraishi, 2013; Tian et al., 2013; Tansug et al., 2014 and Khan et al., 2015). The groups of compounds of interest here include two groups: thioureas and quinones.

The mechanism of corrosion inhibition by thioureas has not been elucidated comprehensively despite of the fact that their complexes have been extensively investigated by X-Ray Crystallography (Taylor et al., 1974 and Bowmaker et al., 2008) and electrochemistry both in aqueous (Cofre and Bustos, 1994) and nonaqueous conditions (Chuaysong et al., 2008). It is well known that thiourea forms formamidine disulfide on copper surface and greater concentrations cause corrosion due to complex formation (Mostafa et al., 2002 and Gomez et al., 2009).

Quinones and similar ring compounds have been found to have interactions with copper and exhibit corrosion inhibitions via adsorption (Sayak et al., 2008), mainly because of their roles in biological cofactors (Wang et al., 2011). Quinones can also be used as a helper for the inhibition of corrosion on metal surfaces by hydrazines (US Patent 3551349 A.). It has also been proved that quinones can inhibit corrosion of mild steel and iron (Muralidharan et al., 1995; Jeyaprabha et al., 2005 and Musa et al., 2012 and). To investigate their behavior, their insolubility causes the use of ionic liquids (Puerto et al., 2013).

Due to the fact that there are quite a few corrosion studies in nonaqueous conditions, the corrosion inhibition behaviors of the two groups of compounds in nonqueous solvents are the topic to be focused here. Aqueous condition might resemble the real situation; however, it can have the effect of hydrogen and oxygen species on the behavior of the inhibitors. Furthermore, there are number of electrochemical studies in nonaqueous conditions which should shed some lights in understanding copper corrosion inhibition by thioureas and ring compounds as well as their complexation mechanism.

1.2 Background

1.2.1 Chemical and physical properties of copper

Copper is a chemical element with atomic number of 29 and symbol as “Cu”. It a ductile metal with high electrical and thermal conductivity, mechanical workability and excellent corrosion resistance in atmospheric exposure conditions. This metal has been used extensively in marine application and constructive material for piping, tubing, condensers, conductor as well as a building material (Sudheer and Quraishi, 2013; Lui et al., 2015 and Melchers, 2015). The physicochemical properties of copper are summarized in Table 1-1.

Table 1-1 Summary of some relevant physicochemical properties of copper

Atomic number	29
Electronic configuration	[Ar] $3d^{10}$ $4s^{1}$
Standard atomic weight	63.546 g mol^{-1}
Density (near room temperature)	8.96 g cm^{-3}
Melting point	1084 °C
Boiling point	2562 °C (sublimes)
Heat of fusion	13.26 kJ mol^{-1}
Heat of vaporization	300.4 kJ mol^{-1}
Heat capacity (25 °C)	24.440 J mol^{-1} K^{-1}
Oxidation states	+1, +2, +3, +4
Electronegativity	1.90 (Pauling scale)
Atomic radius	128 pm
Covalent radius	132 pm
van der Waals radius	140 pm
Electrical resistivity (20 °C)	16.78 nΩ·m
Mohs’ hardness	3.0

Source: http//en.wikipedia.org/wiki/Copper

1.2.2 Corrosion basic

Corrosion is the undesirable deterioration of materials (usually a metal) due to electrochemical reactions with their environments. When the surface of metal is exposed to an electrolyte usually occupies sites for an oxidation (anodic reaction) that produces electrons in the metal at less stable sites. The anodic reaction is the dissolution of the metal to corresponding metal ions (Jones, 1995). A typical anodic oxidation of metal can be expressed by the following half-cell reaction (equation *(1)*).

$$M \rightarrow M^{n+} + ne- \qquad \ldots\ldots\ldots\ldots(1)$$

A reduction half-reaction (cathodic reaction) consumes the electron produced by the anodic reaction. The following three reactions represent cathodic reactions involved in corrosion process (Jones, 1995), at the metal/solution interface are:

(1) aerated neutral and alkaline environments

$$O_2 + 2H_2O + 4e^- \rightarrow 4OH^- \qquad \ldots\ldots\ldots\ldots(2)$$

(2) aerated acidic in the presence of oxygen environments

$$O_2 + 4H^+ + 4e^- \rightarrow 2H_2O \qquad \ldots\ldots\ldots\ldots(3)$$

(3) hydrogen evolution or acidic environments

$$2H^+ + 2e^- \rightarrow H_2 \qquad \ldots\ldots\ldots\ldots(4)$$

1.2.3 Corrosion kinetics

1.2.3.1 Overpotential *(η)*

η is the difference between electrode potential with that when no current passing through it and with that when a current passing. η can be measured by

forcing the extra energy to drive a reaction at the electrode. η increases with increasing current density (Bard and Faulkner, 2000). When two different metals are connected, the corrosion potential (E_{corr}) that occurs in this case is associated with the reversal potentials of the anodic and cathodic reaction. The differentiation of the reversal potential (E_{eq}) and resultant potential (E) is referred to polarization and it can be represented in terms of η as shown in equation *(5)*:

$$\eta = E - E_{eq} \qquad \ldots\ldots\ldots\ldots (5)$$

The polarization is considered to be cathodic, when the anodic processes on the electrode are triggered by moving the potential negative direction and when the anodic processes are triggered by changing the potential to positive direction the polarization is considered to be anodic.

1.2.3.2 Concentration polarization

Concentration Polarization is the part of polarization resulting from changes in electrolyte concentration adjacent the electrode surface as illustrated in Figure 1-1. When a chemical species cooperating in a corrosion process is in short supply, the mass transport of that species to the surface can become rate controlling. The cathodic reaction rate is limited by the concentration of dissolved (Shreir et al., 1994 and Roberge, 2008).

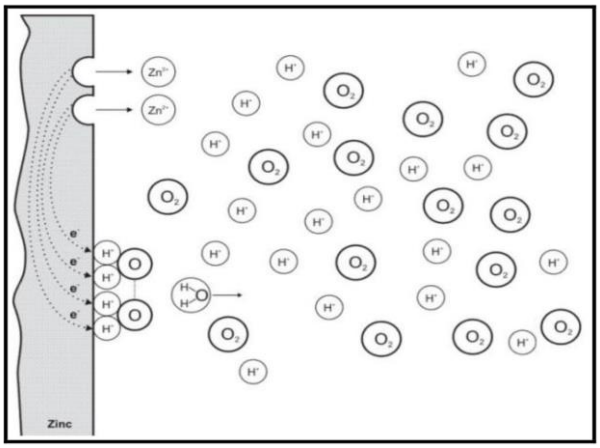

Figure 1-1 Polarization resulting when the concentration of electrolyte adjacent the surface of electrode changes (Roberge, 2008)

The rate of corrosion can be dominated by limiting the transportation of mass to the electrode surface. Figure 1-2 showed that the transportation of species to the electrode surface is relating to diffusion, migration and convection forces (Roberge, 2008). In the case of no electric field flowing, the migration term is negligible, there is only effect from ionic species. In stagnant condition, the convection force is limited.

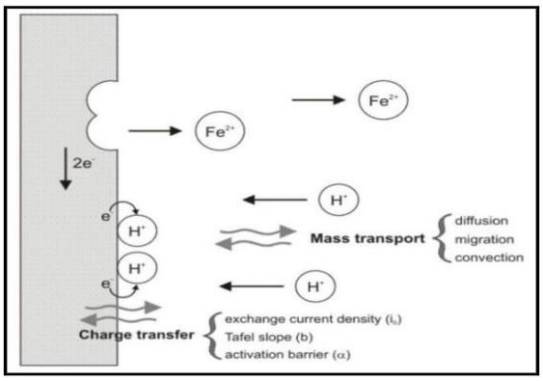

Figure 1-2 The processes occurring at an electrochemical interface (Roberge, 2008)

1.2.3.3 Butler-Volmer equation

Butler-Volmer equation is one of the most basic electrochemical kinetics used to describe how the electric current on an electrode depends on the electrode potential, giving that both an anodic and a cathodic reaction occur on the same electrode (Roberge, 2008):

$$j_{reaction} = j_0 \left\{ \exp(-\beta \frac{nF}{RT} \eta_{reaction}) - \exp((1-\beta) \frac{nF}{RT} \eta_{reaction}) \right\} \quad \text{.....(6)}$$

Where j_{reaction} is the anodic or cathodic current, β is the charge transfer barrier for the anodic or cathodic reaction, n is the number of participating electrons, F is Faraday constant 96485 C/(mole of electrons), R is the universal gas constant (8.314 $mol^{-1}K^{-1}$) and T is the absolute temperature (298 K) and.

Where η_{reaction} is cathodic, the second term in the Butler-Volmer equation becomes negligible and equation *(6)* can be expressed as:

$$j_{reaction} = j_{cath} = j_0 \exp(-\beta n F\, \eta_{reaction}/RT) \quad \text{.....(7)}$$

$$\eta_{reaction} = \eta_{cath} = b_c \log_{10}(j_{cath}/j_0) \quad \text{.....(8)}$$

where b_c is the cathodic Tafel slope represented in equation *(9)*

$$b_c = -2.303RT/\beta nF \quad \text{.....(9)}$$

that can be obtained from the slope of a plot of η versus log current density. From the intercept as shown in Figure 1-3, j_0 can be obtained.

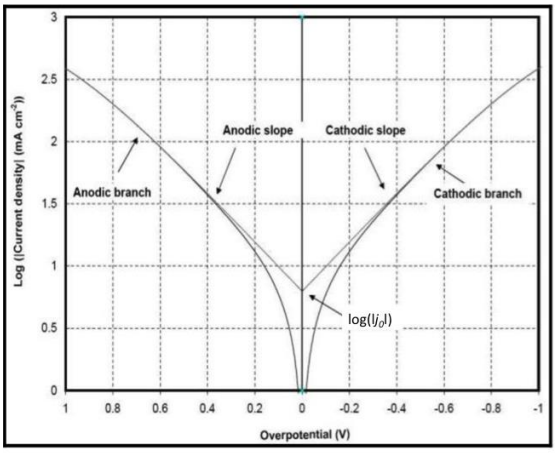

Figure 1-3 Plot of overpotential (η) versus log current density (j) (Roberge, 2008)

Similarly, when η_{reaction} is anodic, the anodic current density (j_{anode}) can be represented by equation and its logarithm, with b_{anode} obtained by plotting η_{reaction} vs. log $|j|$:

$$j_{reaction} = j_{anode} = -j_0 \exp\left((1-\beta)\frac{nF}{RT}\eta_{reaction}\right) \quad \text{.....(10)}$$

$$\eta_{reaction} = \eta_{anode} = b_{anode} \log_{10}\left(\frac{|j_{anode}|}{j_0}\right) \quad \text{.....(11)}$$

$b_a = -2.303RT/\beta nF$ ……*(12)*

1.2.4 Copper dissolution

Although copper is a relatively noble metal and is more stable in the atmosphere, it also can form ions in water. Copper forms two cations by losing electrons (e^-), as in equations *(13)* and *(14)*. The process of losing electrons is attributed to as oxidation by oxygen which often picks up the electrons (a reduction process), see equation *(15)*. Copper can thus react with oxygen in water as shown by equations *(16)* and *(17)* (Oliphant, 2010).

$Cu_{(s)} \leftrightarrow Cu^+ + e^-$ .....*(13)*

$2Cu_{(s)} \leftrightarrow Cu_2^+ + 2e^-$ ……*(14)*

$O_2 + 4e^- \leftrightarrow 2O_2^-$ ……*(15)*

$2Cu_{(s)} + ½O_{2(aq)} \leftrightarrow Cu_2O_{(s)}$ ……*(16)*

$Cu_{(s)} + ½O_{2(aq)} \leftrightarrow CuO_{(s)}$ ……*(17)*

The Cu^+ and Cu^{2+} ions can exist on their own in solution and they can also form complexes with a variety negatively charged ions such as chloride (Cl^-), hydroxide (OH^-), sulphate (SO_4^{2-}) and carbonate (CO_3^{2-}) ions. Together with oxygen, these are all parts of the main corrosion products found at bridge structure, on copper roofs, and in copper pipes (Oliphant, 2010).

1.2.5 Corrosion inhibitors

A corrosion inhibitor is a substance when added in a small amount to decrease the deterioration rate of materials in corrosive environment. Over the years a number of inorganic compounds have been used as corrosion inhibitors for different materials and different environments. However, a number of effective inorganic inhibitors such as chromate, phosphate, molybdate and nitrites will be abandoned due to their toxicity (Tian et al., 2013). Thus there is a need for studying and developing corrosion inhibitors that are effective and environmentally friendly.

Because of the toxicity of inorganic inhibitors, organic inhibitors are most likely to meet those requirements.

1.2.6 Organic corrosion inhibitors

The use of organic corrosion inhibitors is one of the most extensive methods of protecting corrosion of metal. Organic inhibitors can strongly adsorb on the surface of metal to form a protective layer; consequently, reduces the dissolution of the metal into the electrolyte. The polar function is usually regarded as the reaction center for the establishment of the adsorption process due to the polar functional groups such as oxygen, nitrogen, oxygen, sulphur and phosphorous atoms in the molecular structure can donate electrons to the metal. A number of organic compounds have been tested and exhibit inhibitive properties such as carboxylic acids, urea, amines, azole, alkaloid and other nitrogen containing compounds (Rajkumar and Sethuraman, 2014).

The change in corrosion potential on addition small amount of the inhibitor can be used to identify whether the anodic or cathodic reaction is retarded. When the corrosion potential is moved to the positive direction (anodic control), the inhibitor is referred to as an anodic inhibitor. On the other hand, when the corrosion potential is moved to negative direction (cathodic control), the inhibitor is referred to as a cathodic inhibitor. When the inhibitor affects both the anodic and cathodic processes (little change in the corrosion potential) it is referred to as a mixed inhibitor. Figure 1-4 shows how these changes would be reflected in polarization curves (Gil, 2013).

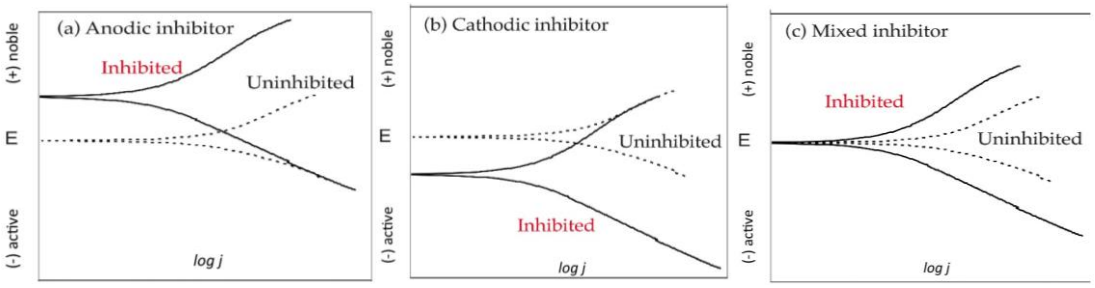

Figure 1-4 The expected change in potentiodynamic polarization curves due to addition of anodic, cathodic and mixed inhibitors (Gil, 2013)

1.2.7 Techniques for analysis of corrosion inhibitors

The most useful techniques for analyzing, the performance corrosion inhibitors are electrochemical measurements such as potentiodynamic polarization and electrochemical impedance spectroscopy. In addition, cyclic voltammetry and spectroscopy techniques are used to describe the reaction and complexation between inhibitor and metals on corrosion process (Sudheer and Quraishi, 2013 and Rajkumar and Sethuraman, 2014). In corrosion field, quantum chemical calculations are used for determination of the molecule and electronic structures. Furthermore, this method can also be used to explain the reactivity between the corrosion inhibitor and metal.

1.2.7.1 Potentiodynamic polarization

Potentiodynamic polarization is an electrochemical technique used for studying corrosion of sample by scanning the sample potential from below to above E_{corr} and measure a current response. The rang of the potential scan is often several hundred millivolts. Data is usually plotted as log of current density (j; x-axis) versus potential (E; y-axis), as shown in Figure 1-5.

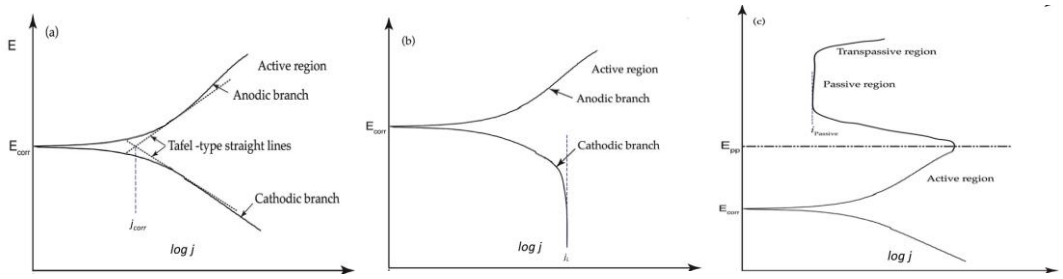

Figure 1-5 Schematic diagrams of polarization curves. (a) Activation controlled anodic and cathode reactions, with straight lines added to demonstrate Tafel extrapolation method for estimation of j_{corr} and E_{corr} (b) Cathodic branch profile exhibits a constant/limiting current typical of diffusion-limited process. (c) Anodic branch profile is that expected for a substrate undergoing passivation (Gil, 2013)

Given that the polarization curve exhibits an appropriate profile, demonstrative of activation controlled cathode and anodic reactions (linear regions as the potential is polarised away from E_{corr}), corrosion current density (j_{corr}), and thus corrosion rate, can be calculated from Tafel extrapolation of the cathodic and the cathodic branches of the curves (as illustrated in Figure 1-5 (a)). This method presumes that the cathodic and the anodic reactions present Tafel behaviour, i.e.

$$E = a + b \log j \qquad \text{……(18)}$$

where a is constant, b is referred to as the Tafel slope. Equation *(18)* is derived from the Butler-Volmer equation, which describes how electrode current depends upon potential (Bard and Faulkner, 2000).

From the polarization curve, additional details about interfacial electrochemistry such as the presence of diffusion controlled reactions and substrate passivation can be obtained. For instance, in Figure 1-5 (b), the cathodic profile reveals that the cathodic reaction is diffusion limited, i.e. a constant/limiting current (j_L) is noticed as the potential is varied. Figure 1-5 (c) presents a polarization profile consistent with a substrate undergoing coating upon anodic polarization. At potentials more positive than E_{corr} (anodic curve), the current reaches a maximum at the passivation potential (E_{pp}) and drops away. The low current is maintained as the potential is raised, until the film is broken down due to pitting (Lorenz, 1981).

Based on the corrosion current density data, the inhibition efficiency (*IE*) can be calculated according to equation *(19)*:

$$IE(\%) = \frac{j_{corr} - j_{inh}}{j_{corr}} \times 100 \qquad \text{……(19)}$$

where the j_{corr} and j_{inh} are the corrosion current density without and with inhibitor, respectively.

A limitation of the Tafel method for corrosion determination is the rather large potential expedition away from E_{corr}, the sample surface could be modified. Therefore, if the determination is to be repeated, the sample needs to be re-prepared and allowed to stabilize in the electrolyte until a steady E_{corr} of sample is reached. Consequently, the Tafel extrapolation method is not agreeable to studies requiring pseudo continuous measurements of j_{corr} (Gil, 2013).

1.2.7.2 Electrochemical impedance spectroscopy (EIS)

EIS is an electrochemical technique has been developed by corrosion scientists to study the response of corroding metals. This technique is employed to obtain information on corrosion by applying a sinusoidal potential of widely varying frequency as a function of time, as in equation *(20)* to working electrode and measure a current response (Jones, 1995), see equation *(21)*.

$$E(t) = E_0 \sin \boldsymbol{\omega} t \qquad \text{……(20)}$$

$$I(t) = I_0 \sin(\boldsymbol{\omega} t + \Phi) \qquad \text{……(21)}$$

where $E(t)$ is potential at time t, E_0 is amplitude, ω is radial frequency = $2\pi f$, f is frequency, $I(t)$ is current response at time t, is shifted in phase, Φ phase-shift and I_0 is amplitude

From Ohm's Law, the impedance of the system can be expressed as:

$$Z = \frac{E(t)}{I(t)} = \frac{E_0 \sin \boldsymbol{\omega} t}{I_0 \sin(\boldsymbol{\omega} t + \Phi)} = Z_o \frac{\sin \boldsymbol{\omega} t}{\sin(\boldsymbol{\omega} t + \Phi)} \qquad \text{……(22)}$$

where Z and Z_o are impedance and magnitude respectively.

With Eulers relationship, see equation *(23),* the impedance is then represented as a complex function, as in equation *(24)*.

$$exp(j\Phi) = cos\Phi + jsin\Phi \quad \text{……(23)}$$

$$Z(\omega) = Z_o cos\Phi + j\, Z_o sin\Phi \quad \text{……(24)}$$

where Φ is real number and j is imaginary unit.

In the electrochemical literature, real and imaginary components of electrochemical impedance are usually marked as Z' and Z'' respectively and The impedance ($Z(\omega)$) can be expressed in Nyquist plots of $Z''(\omega)$ as a function of $Z'(\omega)$, as in equation *(25)*.

$$Z(\omega) = Z'(\omega) + Z''(\omega) \quad \text{……(25)}$$

The plot for a simple parallel-connected resistance-capacitance circuit is shown in Figure 1-6.

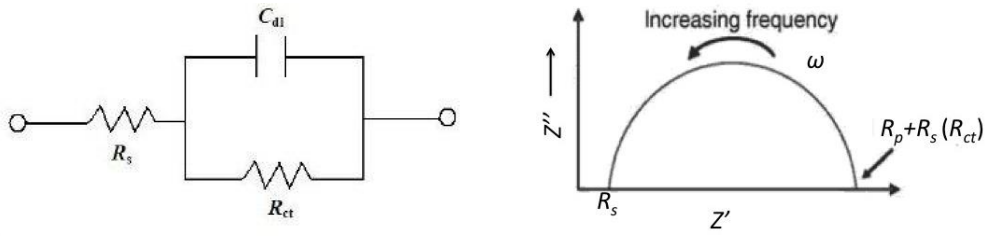

Figure 1-6 Data display for electrochemical impedance spectroscopy for a corroding electrode simulation by parallel-connected resistance R_p and capacitance C

This circuit represents a simple corroding surface under activation control. With increasing frequency in a counterclockwise direction, the Nyquist plot shows a semicircle, leaving only the solution resistance, R_s. At low frequency, Z'' again disappears, leaving a sum of R_s and the polarization resistance, R_p (Jones, 1995). Based on the charge transfer resistance (R_{ct}) data, the inhibition efficiency can be calculated according to equation *(26)*:

$$IE\% = \frac{R_{ct} - R_{ct}^{0}}{R_{ct}^{0}} \times 100 \qquad \text{……(26)}$$

where R_{ct} and R^{0}_{ct} are the charge transfer resistance with and without inhibitor, respectively.

1.2.7.3 Fourier transform infrared spectrometry (FTIR)

Fourier transform infrared spectrometry (FTIR) is a spectroscopic technique employed to establish the chemical structure of a sample molecule. This technique can also be used in qualitative and quantitative analysis by passing IR energy from a glowing black body through the interferometer where the beam is maneuvered thought the sample. When the beam then hits the sample, the sample will absorb IR energy at specific frequencies, the absorption ability of the sample depends on the function groups of the sample. After that the beam reaches the detector then the signal from detector is converted to be a digital signal to show on the screen in form of IR spectrum. The obtained spectrum can be further employed to identify the characteristics of the sample. (http://www.mmrc.caltech.edu/FTIR/FTIRintro.pdf, 2001). These processes can be seen in Figure 1-7.

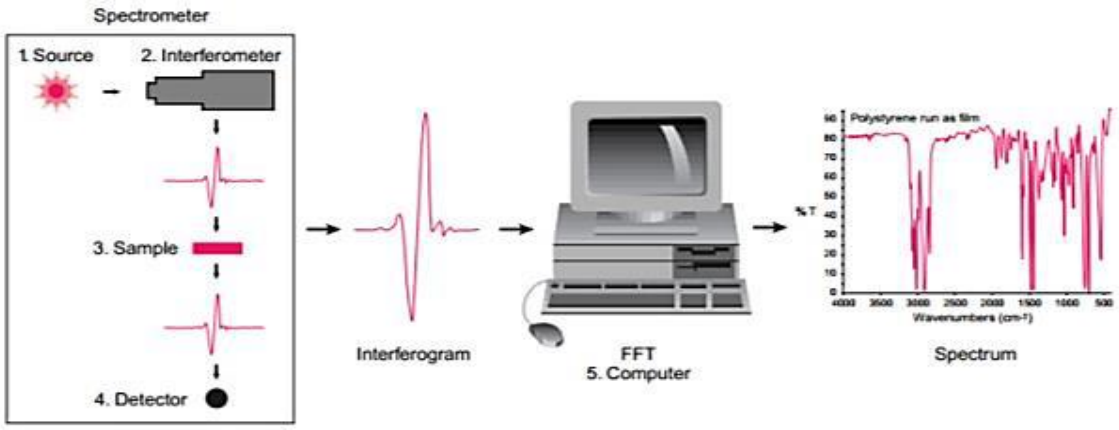

Figure 1-7 Process depicting FTIR analysis (http://www.mmrc.caltech.edu/FTIR/ FTIRintro.pdf, 2001)

Generally, the obtained IR spectrum consists of absorption peaks that involved to a vibration frequency between the bonds in the molecule. It can be used to identify the components (functional groups) of the sample because each functional group can produce just one adsorption peak, and the size of the peaks can also be used to determine the amount of analyte in the sample. (http://www.mmrc.caltech.edu/FTIR /FTIRintro.pdf, 2001).

1.2.7.4 UV-visible spectrophotometry

UV-visible spectrophotometry is a very effective and useful technique for the quantitative and qualitative measurement purposes. By passing electromagnetic radiation between 190 nm to 800 nm through the sample solution, specific wavelength is absorbed. The amount of light absorbed by a sample depends on the thickness of the sample, the concentration of analyte in the sample and particular group in the molecule which can absorb the light, for instance, the compound having double or triple bond group; C=C, C≡C, nitroso, nitro, azo and carbonyl. The absorbed energy will stimulate an electron from ground state to excited state with the wavelength where the analyte absorb the light. The absorption capacity of the analyte can be enhanced by attaching further more groups such as OH^-, NO_2^- and $N^+H_3CH_3$ on the absorbing group. These species also affect to change absorption maximum from lower to a longer wavelength, known as red shift (Soomro, 2009).

Normally, most of metal complexes are coloured due to an electron is transferred from ligand to metal and may transfer electron from metal to ligand and absorb the light in the visible spectrum. Most transitions are colored due to d-d transitions (Figure 1-8) which produces intense absorption peaks of analytical scope. In the quantitative analysis, the concentration of analyte in the sample solution is calculated by plotting absorbance versus concentration through a calibration graph (Soomro, 2009).

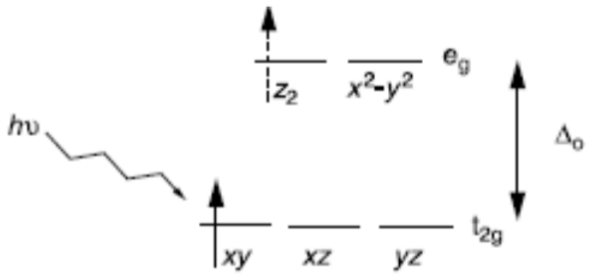

Figure 1-8 Metal complexes d-d transitions for the colour absorption (Soomro, 2009)

1.2.7.5 Cyclic voltammetry (CV)

CV is a widely used electroanalytical technique for acquiring qualitative information such as the study of redox potential of the electroactive species, for understanding reaction intermediates. In particular, this technique provides data about the kinetics, thermodynamics of redox processes as well as the adsorption process. This technique is performed by linearly scanning the electrode potential in an unstirred solution with a triangular potential waveform (Liu, 1997) as shown in Figure 1-9.

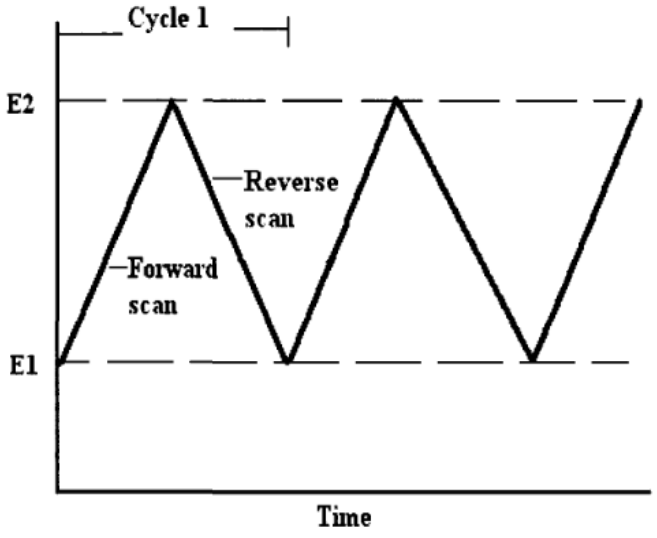

Figure 1-9 Cyclic voltammetry potential waveform (Wang, 2000)

In cyclic voltammetric measurement, the cycle of ramp potential can be duplicated as many times as needed. During the scan, the current resulting from the applied potential is measured by potentiostat. The current is plotted versus the applied potential, and the result is termed a cyclic voltammogram (Liu, 1997).

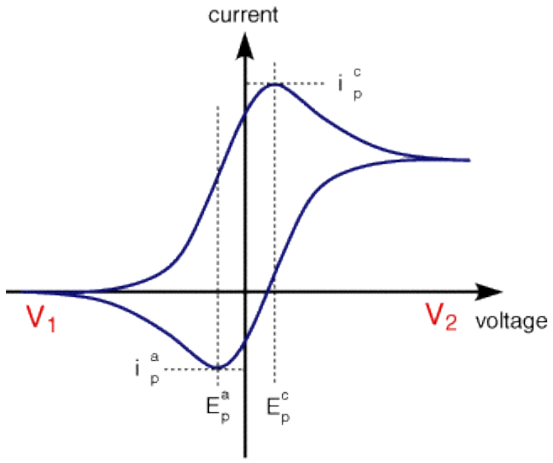

Figure 1-10 A typical cyclic voltammogram of current versus potential (Wang, 2000)

Figure 1-10 shows the important parameters that obtained from cyclic voltammogram are the magnitudes of anodic peak current (i_p^a), the cathodic peak current (i_p^c), the anodic peak potential (E_p^a) and cathodic peak potential (E_p^c).

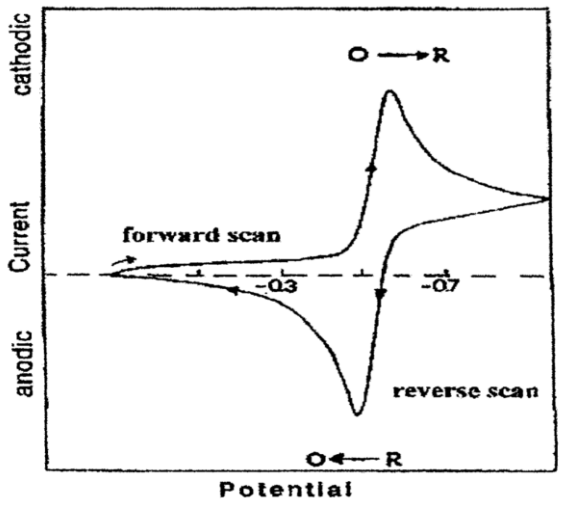

Figure 1-11 A typical cyclic voltammogram in the case of a reversible O + ne^- <=> R redox process (Wang, 2000)

Figure 1-11 illustrates the basic shape of the current versus potential response for a reversible redox couple by a single scan. At the initial stage, the bulk solution contains only the oxidized form "O". The first half cycle is scanning the potential to negative direction where no reduction occurs. As the redox potential is accesses, a cathodic current begins to increase (O is converted into R), until a peak is reached. The second half cycle is reversing scan the potential after traversing the potential region. During this process, an anodic current is rising (R is reconverted into O). The cyclic voltammogram documented in the cast of a reversible electrochemical reaction has outlined characteristics (Liu, 1997):

1) The separation between the peak potentials is written by:

$$\Delta E = E_p^a - E_p^c = \frac{0.059V}{n} \qquad \text{……(27)}$$

Where n is the number of the electrons transferred in the redox reaction.

2) The position of cathodic and anodic peaks does not change as a function of sweep rate.

3) The ratio of forward-to-reverse peak currents is equal to one:

$$\left|\frac{i_p^a}{i_p^c}\right| = 1 \qquad \text{……(28)}$$

4) The peak currents are proportional to the square root of the sweep rate v,

$$i_p^a \; and \; i_p^c \alpha \sqrt{v} \qquad \text{……(29)}$$

5) The effect of scan rate on the peak current i_p is described by the Randle-Sevcik equation, i_p depends not only on the concentration and diffusional properties of the electroactive species but also on scan rate.

$$i_p = 0.4463nFAC\left(\frac{nFvD}{RT}\right)^{\frac{1}{2}} \qquad \text{……(30)}$$

Where i_p is current maximum in amps, A is electrode area in cm^2, F is Faraday Constant in $C\ mol^{-1}$, D is diffusion coefficient in cm^2/s, C is concentration in mol/cm^3, v is scan rate in V/s, R is Gas constant in $J\ K^{-1}\ mol^{-1}$ and T is temperature in K

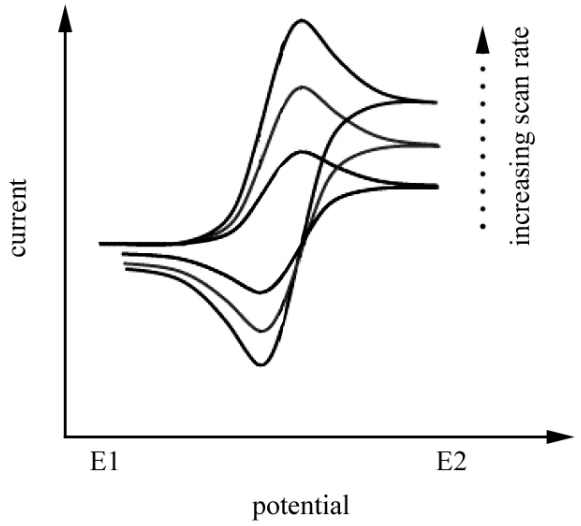

Figure 1-12 Effect of altering sweep rate on the current response for reversible electron transfer processes (Collins, 2012)

Figure 1-12 shows the effect of altering sweep rate on the current response for a reversible electron transfer processes (the system is one that has fast electron transfer kinetics). Each curve has the same feature but the total current increases with increasing scan rate. This effect can be attributed the growth of the diffusion layer and the time taken to record the scan. At low sweep rate, the longer a scan takes to run, the growth of diffusion layer is high. Thus in the case of a slow voltage sweep the flux to the electrode surface is smaller than the flux to the electrode surface at fast voltage sweep. At high sweep rate, the magnitude of the current response is higher in comparison to low sweep rates due to the current response is directly proportional to the flux to the electrode surface. The term irreversible electron

transfer reaction refers to the electron transfer kinetics are slow in comparison with the reversible system, more over potential will be required for facilitating electron transfer. The increase in current as a result of oxidation is observed at higher potential values than those observed in the case of the reversible system as shown in Figure 1-13. For a quasi-reversible electron transfer reaction, the electron transfer reaction is neither limiting, but somewhere in between (Liu, 1997).

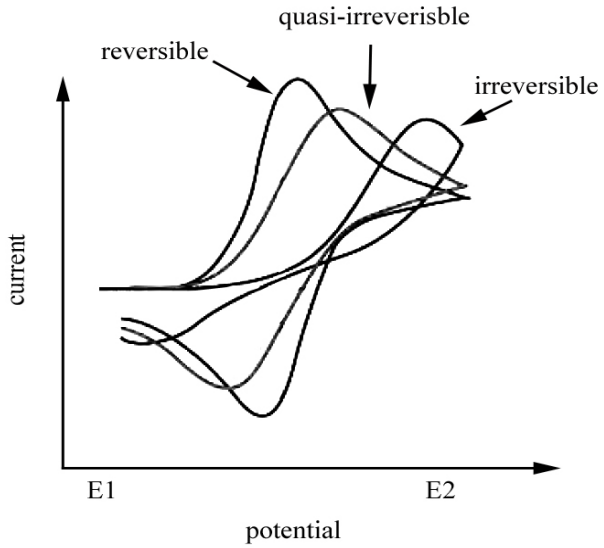

Figure 1-13 Cyclic voltammogram for reversible, quasi-reversible and irreversible electron transfer processes (Collins, 2012)

In the case of irreversible and quasi-reversible electron transfer reaction the surface concentration of species at the electrode surface is affected by both the mass transport and the electron transfer rates (Collins, 2012). The peak high obtained from these processes does not increase as a function of the square root of the sweep rate and the peak positions are dependent on the scan rate, which is not observed for reversible process.

1.2.7.6 Scanning electron microscopy (SEM)

SEM is a type of electron microscope that produces surface images of a specimen on a microscope level by scanning it with a focused beam of high energy electrons in an optical column. The electrons emitted by the beam then interact with atoms on the surface of the specimen, producing various signals to obtain information about the sample's surface topography. Generally, SEM micrograph of the surface of specimen is normally represented as a 2D image. This microscope has a maximum magnification of about 30,000X with a spatial resolution range from 50 to 100 nm. This technique is considered to be non-destructive technique (http://serc.carleton.edu/research_education/ geochem-sheets/techniques/SEM. html, Dec. 22, 2014.).

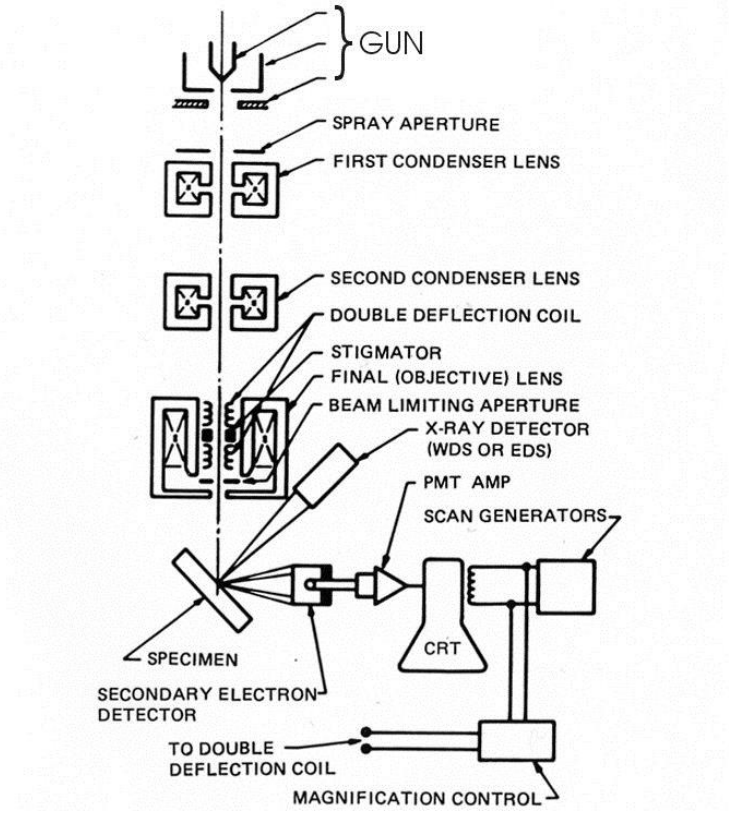

Figure 1-14 Schematic of the Scanning Electron Microscope (http://serc.carleton.edu/research_education/ geochem-sheets/techniques/-SEM. html, Dec. 22, 2014.).

The apparatus inside the SEM instrument are shown in Figure 1-14. An electron beam from a beam gun is scanned across the surface of the specimen. A column containing electromagnetic lenses is employed to focus the beam towards the specimen. When the beam hits the specimen, backscattered and secondary electrons are ejected from the surface of the specimen. A detector collects these electrons and converts them to a signal that can be displayed as a picture.

In corrosion field, SEM is usually used to identify the adsorption of the inhibitor molecules on the surface of the specimen. Figure 1-15 illustrates an example of a typical SEM images. Figure a and b indicated the illustrates of bare copper surface and film formed on copper surface respectively (Rajkumar and Sethuraman, 2014). In this work, SEM analysis will be used in the same way as Rajkumar and Sethuraman's work.

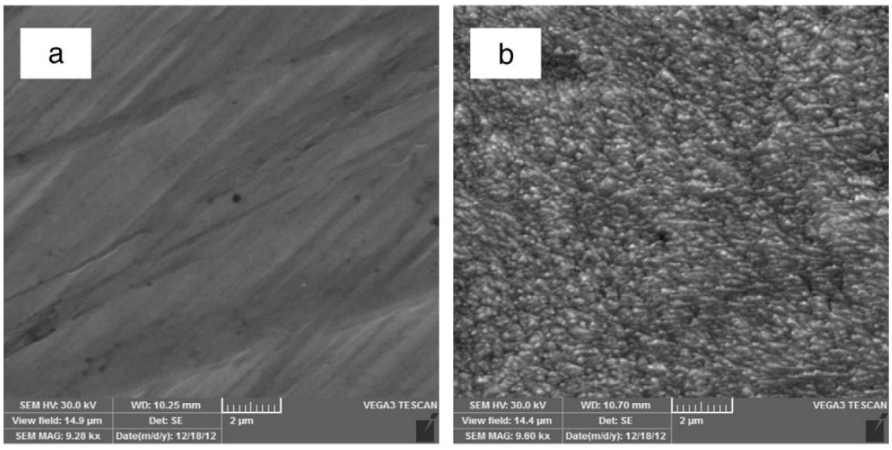

Figure 1-15 Typical SEM images indicating the illustrates of bare metal surface and film formed on metal surface, as indicated figure a and b respectively (Rajkumar and Sethuraman, 2014)

1.2.7.7 Adsorption isotherms

Adsorption of organic molecules on to metal surfaces is normally described by adsorption isotherms. They provide useful insight into the adsorption mechanism of inhibitors on metal surfaces. The adsorption of organic molecules onto metal surfaces can either occur through physisorption or chemisorption (Kar, 2009).

Physisorption is a kind of adsorption mechanism which involves the electrostatic attraction between the adsorbate and the surface. The physisorbed inhibitors can adsorb on the surface quickly but they can also be stripped from the surface easily. Another mechanism of adsorption is chemisorption, a mechanism that involves charge sharing between the adsorbate and the surface. Chemically adsorbed inhibitors interact more slowly than physically adsorbed inhibitors but the bond formed in chemisoption is stronger than the intermolecular forces (Van der Waals forces) in physical adsorption. Therefore, the chemically adsorbed inhibitors are effective.

In this research, three different adsorption isotherms are used to describe the equilibrium relationship between the concentration of inhibitor on copper surface and that one in bulk solution. Three adsorption isotherms using in this research are the Langmuir isotherm, Temkin isotherm, and Flumkin isotherm which are further explained as follows.

Langmuir isotherm

Langmuir isotherm is used for description of a monolayer adsorbate on the adsorbent, the adsorbed molecule occupies a site, and after that no further addition adsorption takes place (Piccin et al., 2011). Langmuir isotherm is given by

$$\frac{C}{\theta} = \frac{1}{K} + C \qquad \text{……(31)}$$

where C is the concentration of inhibitor, θ is the degree of surface covered and K is the adsorption equilibrium constant.

A plot of C against C/θ provides a linear relationship where the slope is unity and the constant $1/K$ (Nwabanne and Okafor, 2012), large adsorption equilibrium constant refers to strong adsorption of adsorbate (Moreno-Pirajan, 2011).

Freundlich isotherm

Freundlich isotherm is generally applied to describe the multilayer adsorption with interaction between adsorbed molecules, adsorption affinities and heart are non-uniform distribution over the heterogeneous surface (Foo and Hameed, 2010). Freundlich isotherm is given by

$$log\theta = logK + nlogC \qquad \text{……(32)}$$

where *K* and *n* are constants for a given adsorbate and adsorbent at a particular temperature, which can be obtained by plotting of log θ against log *C*. From the intercept of this equation the value of *K* can be obtained (Anees, 2008).

Temkin isotherm

Temkin isotherm considers that heat of adsorption of all molecules in the layer would decreases linearly with increasing coverage of the adsorbent on surface. The adsorption is distinguished by a uniform distribution of binding energies. (Piccin et al., 2011). Temkin isotherm is given by

$$\theta = -\frac{2.303logK}{2a} - \frac{2.303logC}{2a} \qquad \text{……(33)}$$

where *a* is the attractive parameter and 2.303 is the conversion factor.

A plot of θ against log *C* provides a linear relationship where the slope is $-2.303/2a$ and the intercept is $-2.303\ logK/2a$. To prove the repulsion exists in the adsorption layer, "*a*" should be negative (Nwabanne and Okafor, 2012).

1.2.7.8 Gibbs free energy

The standard Gibbs free energy of adsorption (ΔG^{o}_{ads}) is used to verify possible adsorption mechanisms, physisorption (20 kJmol^{-1} or lower) or chemisorption (40 kJmol-1 or higher). ΔG^{o}_{ads} can be calculated by using *K* value obtained from the adsorption isotherm. ΔG^{o}_{ads} is given by

$$\Delta G^{o}_{ads} = -RTln(19.147K_{ads}) \quad \text{……(34)}$$

where *T* is the temperature (K), *R* is the universal gas constant and 19.147 is the concentration in M of acetonitrile solvent. (Moreno-Pirajan, 2011 and Deyab, 2015).

1.2.7.9 Quantum chemical studies

Quantum chemical method is computational method for studying the electronic structure and reactivity of interesting molecule (Kraka et al., 2000). In corrosion field, this method is very useful method for studying corrosion inhibition mechanism of inhibitors by observing their possible physical characters which could contribute to corrosion inhibition. Table 1-2 shows some quantum chemical parameters computed by the Gaussian 03 package (Sudheer and Quraishi, 2013), for instance, the energies of the highest occupied (E_{HOMO}), lowest unoccupied (E_{LUMO}) molecular orbitals and dipole moment (D) which were calculated after geometric optimization of the interesting molecule. Highest occupied molecular orbital energy (E_{HOMO}) and lowest unoccupied molecular orbital energy (E_{LUMO}) are used to describe the interaction between the interesting molecule and other species. The HOMO is the outermost orbital containing electrons acts as an electron donor. The LUMO is the innermost orbital that has room to accept electrons acts as the electron acceptor, thus the interaction between molecules is due to an electron transfer between HOMO and LUMO of them (Gece, 2008). By the difference in energy of two frontier orbitals (ΔE), the strength and stability of the molecule in chemical reactions can be predicted.

Table 1-2 Quantum chemical parameters for 4-amino-4H-1,2,4-triazole-3thiol (ATT) inhibitor (Sudheer and Quraishi, 2013)

E_{HOMO} (hartree)	E_{LUMO} (hartree)	ΔE (hartree)	Dipole moment (D)
-0.2342	-0.0282	0.2060	5.46

A small ΔE indicates effectiveness of inhibitor that can donate electrons to unoccupied orbital of a metal, and can also accept free electrons from the metal. Another important parameter is dipole moment (D). D is the product of the total amount of charge with the distance between their centroids. It is used to describe the polarity of molecule (Khadom, 2010), which is the vector sum of individual bond dipole moments in the molecule. It has been reported that, molecules that have large value of D have a tendency to interact with other molecule through electrostatic interactions (Elmsellem et al., 2014) resulting in increasing the corrosion inhibition.

Table 1-3 Mulliken atomic charge density of ATT molecule (Sudheer and Quraishi, 2013)

No	**Atom**	**Charge**
1	N1	-0.289
2	N2	-0.285
3	N3	-0.488
4	N4	-0.545
5	S	-0.098

Charge-based parameters are extensively used as measures of chemical reactivity as well as intermolecular interactions. Mulliken charge distribution is widely employed to estimate net atomic charges of an atom in the molecule. Moreover, net atomic charges are also employed to describe the polarity of the molecule (Khadom, 2010). The Mulliken charge distribution of ATT (Table 1-3 and Figure 1-16) could be observed that nitrogen atom has the highest electron density

implied that the N were the active center, which has strongest ability to bond with metal surface.

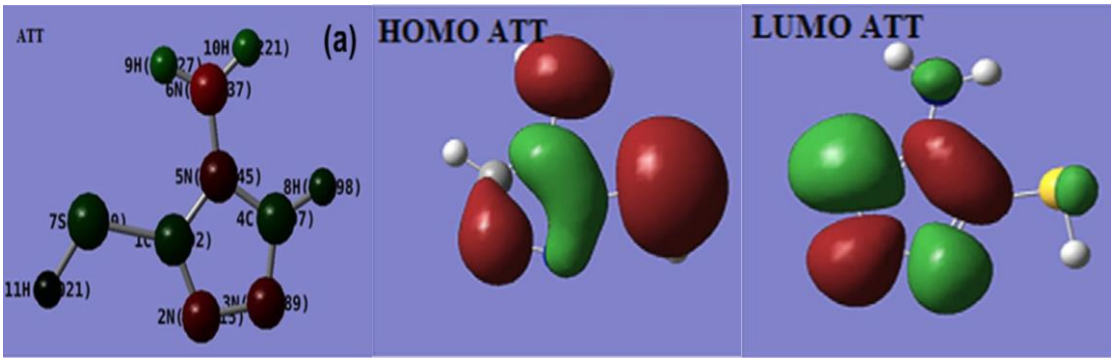

(a) (b) (c)

Figure 1-16 (a) optimized geometry of ATT molecule (b) HOMO energy density of ATT (c) LUMO energy density of ATT molecule (Sudheer and Quraishi, 2013)

1.3 Literature reviews

Copper is a metal that has been used for some 10000 years. Copper acquired its name during the roman era from being mined on Cyprus, Cyprium or Cuprum meaning “metal from Cuprus”. In nature, copper is usually combined with other chemicals in form of copper ores, e.g. covellite (CuS) and chalcocite (Cu_2S). Currently, copper is widely used in a number of fields as a structural component especially in marine systems (Tian et al., 2013). Because of its good corrosion and biofouling resistance, in marine industries copper is used for piping, tubing, heat exchanger and condensers and, at the one time, for sheathing the hull of boats and ships (Melchers, 2015). It is also used to secure safe storage of nuclear waste where copper canisters are proposed barrier (Kazeem et al., 2015). By combining copper with other metals can create different alloys which show different properties such as superior thermal and electrical conductivity, excellent corrosion resistance, wide range of attainable mechanical properties, ease of fabricating and joining and resistance to biofouling. However, copper is susceptible to corrosion in aggressive

media such as oxidizing acids, oxidizing heavy-metal salts, ammonia and environments with high chloride levels.

The use of organic inhibitors is one of the best options for protection against corrosion of metals and their alloys. In particular, some organic inhibitors have been used for the purpose by forming a protective film on metal surface through the presence of polar functional groups including sulphur, nitrogen, oxygen and phosphorous atoms in their molecules, as well as pi electrons especially in heterocyclic ring (Tian et al., 2015). These include amino acids, triazoles, Schiff bases, thioureas, naturally derived extracts, phytate and quinone derivatives. It has been demonstrated that these inhibitors, typically containing sulphur, nitrogen and oxygen as major adsorption centres (Khiati et al., 2011; Behpour et al., 2012; Chen et al., 2012; Hong et al., 2012; Levin et al., 2012; Sun et al., 2012; Hong et al., 2013; Pan et al., 2013 and), although some of them are inadequate to be environmentally friendly and high-efficiency.

1.3.1 Triazole and analogous compounds

As early as 2009, Khalid, (2009) studied corrosion inhibition of copper in hydrochloric acid medium containing N-(2-thiazolyl)-1H-benzotriazole-1-carbothioamide (TBC). Here TBC is a good inhibitor via chemisorption through carbothioamide and thioazolyl groups on the copper surface and this blocks adsorption of oxygen and formation of a prenucleation layer which is the precursor for the formation of oxide. The data obtained from quantum chemical calculations reveal that TBC has higher HOMO, lower LUMO and lower energy gap than BTA (Kim et al’s paper), proving that TBC is better copper corrosion inhibitor compared with BTA.

In 2013, the corrosion inhibition ability of triazole derivatives, namely 4-amino-4H-1,2,4-triazole-3thiol (ATT), 4-amino-5-ethyl-4H-1,2,4-triazole-3thiol (AETT) and 4-amino-5-methy l-4H-1,2,4-triazole-3thiol (AMTT) for copper in hydrochloric acid medium were investigated by potentiodynamic polarization method Sudheer and Quraishi, (2013). The obtained data indicated that all three examined compounds are cathodic type inhibitors, cathodic inhibitors act by slowing the

cathodic reaction itself. Among the studied compounds, ATT was poor inhibitor, while AETT and AMTT were better. AETT gave the best protection of copper in 0.5 M HCl solution. When used as a pretreatment for copper surface, AETT was also the most effective.

The inhibitive effect of two novel non-toxic thiadiazole derivatives such as (5-phenyl-1,3,4-thiadiazole-2-thiol (PTT) and 2-(5-mercapto-1,3,4-thiadiazole-2-yl)-phenol (MTP) as a corrosion inhibitor for copper in sodium chloride medium were tested using weight loss and electrochemical measurements (Tain et al., 2013). The obtained results reveal that both cathodic and anodic current densities were decreased by the addition of these compounds, charge transfer process was suppressed by adsorption on copper surface. The adsorption of these compounds obeys Langmuir isotherm. The results obtained from SEM couple with EDX reveals that these compounds were strongly adsorbed on copper surface via formation of thiazole-copper complex.

Kim et al., (2014) studied effect of nitrogen atoms of benzotriazole (BTA), (N=3) and its derivatives included indole (N=1), indazole (N=2), benzoimidazole (N=2), and 1H-benzotriazole-methanol (BTA-MeOH), (N=3) on the corrosion of copper in sulfuric acid. The testing showed that the additives containing three nitrogen atoms (BTA and BTA-MeOH) more effectively inhibited copper corrosion than other BTA-derivatives having fewer nitrogen atoms. Copper deposited with BTA or BTA-MeOH showed 35% reduced grain size by chemisorption thought nitrogen atoms in the azole ring.

Corrosion protection ability of 3-amino-5-mercapto1,2,4-triazole film on copper was studied by using potentiodynamic polarization and EIS. The characterization of this film studied by using FTIR, CV and SEM techniques (Rajkumar and Sethuraman, 2014). Under all conditions, the film formed on copper surface showed significant protection ability in sodium chloride medium. The enhanced corrosion protection ability is due to the film blocks the electron transfer from the solution to copper surface.

1.3.2 Amino acids

The inhibition of deterioration of copper in 0.5 M hydrochloric acid solution by four amino acids included asparagine (Asn), aspartic acid (Asp), glutamic acid (Glu) and glutamine (Gln) has been studied by potentiodynamic polarization and EIS measurements (Zhang et al., 2008). The results from both techniques revealed that all amino acids inhibited the corrosion rate of copper. The corrosion inhibition efficiency of these compounds depends on their molecular structure. It increases in the order: Gln > Asn > Glu > Asp. Gln and Asn exhibits higher inhibiting behavior than Glu and Asp due to their adsorption though more nitrogen atoms. Gln gave higher inhibition efficiency than Asn is due to more methylene in its molecular structure and the inhibition efficiency was found to be increased with Gln concentration up to 93.74% inhibition efficiency at 10 mM. The adsorption of these compounds on copper surface obeys the Langmuir isotherm.

The inhibitive effect of seven amino acids such as alanine (Ala), arginine (Arg), asparagine (Asn), histidine (His), aspartate (Asp), lysine (Lys) and methionine (Met) as a corrosion inhibitor were investigated in gas, water, acetic acid and formic acid phase by quantum chemical calculations with HF/6-31G++ (d, p) and B3LYP/6-31G++ (d, p) methods (Kaya et al., 2015). The results revealed that Arg is the best inhibitor because Arg contain more electron donating group(amine and carboxylicacid) in the structure compared to other amino acids which is in good agreement with experimental results earlier reported in the literature.

Corrosion inhibiting of amino acids such as proline (Pro), phenylalanine (Phe), tyrosine (Tyr) and tryptopane (Try) on the deterioration of copper in 1 M nitric acid was studied using electrochemical polarization and gravimetric measurements (Barouni et al., 2014). Both electrochemical polarization and gravimetric measurements showed that all amino acids have some protective effect against copper corrosion. The corrosion inhibition efficiency of these compounds increases in the order Tyr > Try> Phe > Pro. The Mulliken charge distribution obtained from Quantum chemical calculations reveled that Tyr is the best corrosion inhibitor because of Tyr has more negative atomic charges (N and O atoms)

than other amino acids. These properties enhance the possibility of copper surface being adsorbed more strongly by Tyr.

1.3.3 Schiff bases

Corrosion inhibitor N'-histidine-3-methoxy-salicylidenimine (V-his), N, N'-*o*-phenylen-*bis*(3-methoxy salicylidenimine) (V-oph-V) and N, N'-*p*-phenylen-*bis* (3-methoxy-salicylidenimine) (V-pph-V) on copper surfaces were examined by potentiodynamic polarization and EIS (Li et al., 1999). Results obtained from experimental data showed that all studied Schiff bases act as effective inhibitors for copper in 5% M hydrochloric acid. The corrosion inhibition mechanism of these Schiff bases are adsorption of these compounds by the present of the –C=N- group in their molecules with copper surface. The corrosion resistance was found to be increased with increasing concentration and decreasing temperature.

Behpour and Mohammadi, (2013) studied the inhibition of deterioration of copper in 15% hydrochloric acid containing Schiff bases namely, N-[(Z)-1- phenylemethyleidene]-N-{2-[(2-{ [(Z)-1phenylmethylidene]amino} phenyl)disul-fanyl] phenyl} amine and N-[(Z)-1-(4-methylphenyl)methylidene]-N-{2-[(2-{ [(Z)-1-(4methylphenyl)methylidene]amino} phenyl)disulfanyl]phenyl. The data from potentiodynamic polarization measurement indicated that both Schiff bases have good inhibiting properties with mean inhibition efficiency of 98% at 0.5 mM. Polaization curves revealed that they are anodic-type inhibitors due to their corrosion potentials (E_{corr}) are shifted to more positive values. The adsorption of these Schiff bases on copper surface obeys the Langmuir isotherm and the obtained negative values of ΔG_{ads} indicated that both Schiff bases are strongly adsorbed on the surface. The obtained results from impedance measurements revealed that the charge transfer resistance (R_{ct}) between copper surface and the solution increased with increasing concentration of inhibitors. But it slightly decreased with rising temperature.

The inhibitive effect two bases such as N^1,N^2-didodecy^l-N^1,N^1, N^2, N^2-tetramethylethane-1,2-diaminium bromide (I) and N-(2-hydroxyethyl)-N,N dimethyldodecan-1-aminium bromide (II) as a corrosion inhibitor for copper in 1 M nitric acid were examined using polarization and EIS (Hegazy et al., 2015). Results obtained from experimental data revealed that the inhibition efficiency of both Schiff

bases increased with increasing their concentration, indicating that Schiff bases molecules can adsorb on copper surface and form a protective layer on copper-solution interface. The adsorption of both compounds on the surface obey the Langmuir isotherm and their adsorption are of physisorption type. The maximum inhibition efficiencies (93.9% and 90.8%) were obtained in the presence of 0.001 M of N^1,N^2-didodecyl-N^1,N^1, N^2, N^2-tetramethylethane-1,2-diaminium bromide (I) and N-(2-hydroxyethyl)-N,N-dimethyldodecan-1-aminium bromide (II) respectively.

1.3.4 Thiourea

The inhibiting of thiourea (TU) on the corrosion of Cu-20% Fe alloy in 1.0 M sodium chloride solution was studied using potentiodynamic polarization and EIS (Egamy, 2008). The results showed that thiourea molecules adsorp on alloy surface according to the Langmuir adsorption isotherm and the adsorption mechanism is of strongly chemisorption by sharing electron pairs. Increasing in concentration of thiourea (up to 5 mM), the inhibition efficiency reached 91%.

1.3.5 Naturally derived extracts

Three xanthine derivatives with similar chemical structures such as theophylline, theobromine and caffeine were investigated the corrosion behavior of copper in 0.1 M sulfuric acid by electrochemical techniques (Souza et al., 2012). Both potentiodynamic polarization and EIS measurement revealed that the corrosion rate of copper increased in the presence of theophylline and theobromine and decreased in the presence of caffeine. The corrosion inhibition ability of caffeine increased with increasing the concentration from 1.0 – 10.0 mM. Furthermore, the results obtained from SEM technique indicated the presence of protective layer (caffeine-copper) on the surface. This film covers up to 72% of the total active surface and acts as a barrier for preventing the interaction between copper and the solution.

The inhibition effect of *Curcuma longa* on steel-copper in petroleum waste water solution was investigated using weight loss technique (Khadom et al., 2015). The corrosion inhibition ability was increased with concentration of *C. longa* but decrease at high temperature. The adsorption model of *C. longa*

obeyed the Temkim adsorption isotherm. Addition *C. longa* gave 95.65% protection for copper at 30 ^{o}C.

1.3.6 Phytate

Cyclic voltammetry technique was employed to investigate the adsorption property of phytate in the corrosion of copper in NaOH solution (Wang and He, 2012). The obtained results revealed that phytate has good corrosion inhibition abilities. The inhibition was due to the adsorption of phytate molecules on copper surface consequently decreases the generation of the cupric corrosion products. The results of this study indicate that cyclic voltammetry is an effective method for studying metal corrosion processes.

1.3.7 Quinone derivatives

Inhibition performance seven quinone derivatives namly, 1,4-Benzoquinone (BQ), 1,2-Naphthoquinone ($NQ^{1,2}$), 1,4-Napthoquinone ($NQ^{1,4}$), 2-Methylbenzo-quinone (MBQ), 1,2-Dihydroxy-anthraquinone (AL), 1,2,4-Trihydroxy-anthraquinone (PU) and 1-Amino-4-hydroxy-anthraquinone (AAQ), as corrosion inhibitor for mild steel in neutral aqueous solution was investigated by quantum chemical (Stoyanova and Slavcheva, 2011). The trend of corrosion inhibition ability of these compounds is noticed to be in the order AHAQ > PU > AL > $NQ^{1,4}$ > $NQ^{1,2}$ > MBQ > BQ. Compared with other quinone derivatives, AHAQ greatly improved the corrosion inhibition due to it has the largest dipole moment and lowest ionization potential. The difference in the electronic and geometric structures of ortho- and para-substances causes the different corrosion inhibition effect and action mechanism.

The adsorption properties of polythiophene-anthraquinone sulphonic acid (PTh-AQSA) for mild steel corrosion in 1N hydrochloric acid were investigated by potentiodynamic polarization and EIS techniques (Thirunarayanan et al., 2011). The obtained results showed that corrosion resistance of copper increased with increasing concentration of PTh-AQSA, the inhibition was due to the adsorption of this compound on mild steel surface, which controls both cathodic and anodic

reaction by blocking active sites of mild steel surface. The absorption of PTh-AQSA on the surface obeys Langmuir isotherm.

Muthukumar et al., (2009) reported the inhibiting action of 1-aminoanthraquinone (AAQs) against corrosion of steel (API 5L-X60) in white petrol with water containing 120 ppm of chloride at room temperature by weight loss and electrochemical studies. AAQs is effective corrosion inhibitor with 86% inhibition. The inhibiting action is due to chelate formation between AAQs and steel surface, which inhibits the interaction between steel and the solution.

Umoren and Solomon., (2015) reviewed the effects of three halide ions including chloride ion (Cl^-), bromide ion (Br^-) and iodide ion (I^-) on the corrosion inhibition efficiency of organic inhibitors such as polymers, organic dyes, surfactant, drug etc. on metal corrosion under different experimental conditions. Most of the available data show that when the halide ions was added to the system resulting in increasing of the corrosion inhibition abilities of those organic compounds. The trend of corrosion inhibition ability of the organic compounds in the presence of halide ions is noticed to be in the order $I^- > Br^- > Cl^-$, indicating that the adsorption process of these ions are depend on their atomic radius and electronegativity values, when atomic radius decreases (I^- = 135 pm, Br^- = 114 pm, Cl^- = 90 pm,), the electronegativity increases (I^- = 2.5, Br^- = 2.8, Cl^- = 3.0). Therefore, iodide ion is more inclined to interact with metal other species than the bromide and chloride ions due to its large size and low electronegativity. Although adding the halide ions can cause decrease in corrosion rate, in some cases, the influences of addition of these ions especially chloride ions can also cause increase in corrosion rate rather than decease it. There are a few cases for iodide ions that can cause increase in corrosion rate of metal; therefore, this ion is really remarkable and it is required for further study. From the reports, adding these halide ions can affect corrosion inhibition abilities of organic inhibitors by a strong chemical adsorption on the surface of metal to be the metallic state before the adsorption of organic inhibitor; consequently, increases the surface coverage thereby decreasing the corrosion rate of metal.

As can be seen from the preceding literature review, a number of organic compounds containing N, O and S have been studied as inhibitors for copper corrosion in various environments. Due to the fact that there are quite a few

corrosion studies in nonaqueous conditions, the corrosion inhibition behaviors of dimedone compound in nonqueous solvents are the topic to be focused here. Aqueous condition might resemble the real situation; however, it can have the effect of hydrogen and oxygen species on the behavior of the inhibitors. Furthermore, there are number of electrochemical studies in nonaqueous conditions which should shed some lights in understanding copper corrosion inhibition by dimedone compound as well as their complexation mechanism. The present work aims to study the corrosion inhibition abilities of Thioureas and N, O, S-Ligating Ring compounds as inhibitors for copper in acetonitrile solution by using electrochemical techniques such as potentiodynamic polarization and EIS. In addition, the corrosion inhibition mechanisms of these compounds will also be studied with many difference methods including CV, UV-Vis, FTIR and adsorption isotherms to support those results that obtained from potentiodynamic polarization and EIS techniques. Furthermore, quantum chemical calculations will be employed as an aid to understand how the molecule of inhibitor interacts with copper surface and to predict the inhibition efficiencies of compounds that have similar structure.

1.4 Objectives of this work

The aim of this work is to gain some insight into corrosion process, evaluate corrosion inhibition efficiency of the inhibitors such as thioureas and N, O, S-ligating ring compounds in acetonitrile. For achievement, the steps of study are

1. to investigate the corrosion inhibition effect of these inhibitors on copper in electrochemical techniques, including potentiodynamic polarization EIS,

2. to study the complexation between dimedone and copper by CV, UV-Vis and FT-IR techniques,

3. to characterize the film formed on copper surface by SEM measurement, and

4. to study the interaction between dimedone molecules and copper by Quantum chemical calculation method.

CHAPTER 2

EXPERIMENTAL

2.1 Chemical and reagents

2.1.1 General chemical and solvents

- Thiourea ≥ 99.0%, A.C.S reagent (Aldrich, Switzerland)
- Diphynyl Thiourea ~98.0%, HPLC grade (Fluka, Switzerland)
- Phenyl Thiourea ~90.0%, HPLC grade (Fluka, Switzerland)
- Ethylene Thiourea ~98.0%, HPLC grade (Fluka, Switzerland)
- Xanthone ~97.0%, (Aldrich, Switzerland)
- Xanthene 99.0%, (Fluka, Switzerland)
- Thioxanthone ≥ 98.5%, HPLC grade (Fluka, Switzerland)
- Acridone 99.0%, (Fluka, Switzerland)
- 1,4-Naphthoquinone 97.0%, (Aldrich, Switzerland)
- Dimedone 95.0%, (Aldrich, Switzerland)
- Aniline ≥ 99.0%, (Aldrich, Switzerland)
- Acetic acid ≥ 99.85%, (Aldrich, Switzerland)
- Copper (II) chloride dihydrate 99.0%, (Aldrich, Switzerland)
- Tetrabutylammonium hexafluorophosphase ($TBAPF_6$) ≥ 98.0%, (Fluka,Switzerland)
- Potassium chloride 99.0%, (Aldrich, Switzerland)
- Potassium bromide 99.0%, (Aldrich, Switzerland)
- Potassium iodide 99.0%, (Aldrich, Switzerland)
- Acetone 99.5%, (Lab-scan, Thailand)
- Acetonitrile 99.7%, (Lab-scan, Thailand)

2.1.2 Sample

- Copper foil, thickness 0.25 mm, 99.98%, (Aldrich, Switzerland)

2.2 Instruments

The electrochemical measurements were carried out by Methrom AUTOLAB PGSTAT 100 with GPES software as well as by Methrom AUTOLAB PGSTAT 302N with NOVA software. Quantum chemical calculations were performed with the use of Gaussian 09 package. The molecular structures of dimedone was fully geometrically optimized using the functional RB3LYP DFT formation with electron basis 6-31G (d, p) for all atoms. The Fourier Transform Infrared (FT- IR) spectrum was recorded with Perkin-Elmer FT-IR 783 model in KBr matrix at room temperature. The UV-Vis measurements were carried out by PerkinElmer Lambda 45 model and the surface morphology was analyzed by SEM of Quanta.

2.3 Electrochemical cell set-up

All electrochemical techniques were carried out using a standard three-cell electrode system (Fig 2-1) consisting of a high purity platinum wire as a counter electrode (CE), a silver-silver chloride electrode (Ag/AgCl) as a reference electrode (RE) and a working electrode (WE) which was 99.98% copper coupons with an exposed surface area of 2.075 cm^2 for potentiodynamic polarization and EIS techniques whereas a glassy carbon electrode (GCE, 2 millimeter diameter) for CV technique. The reference electrode was serviced regularly by changing the internal filling solution with a saturated solution of super-purum KCl (99.999+%).

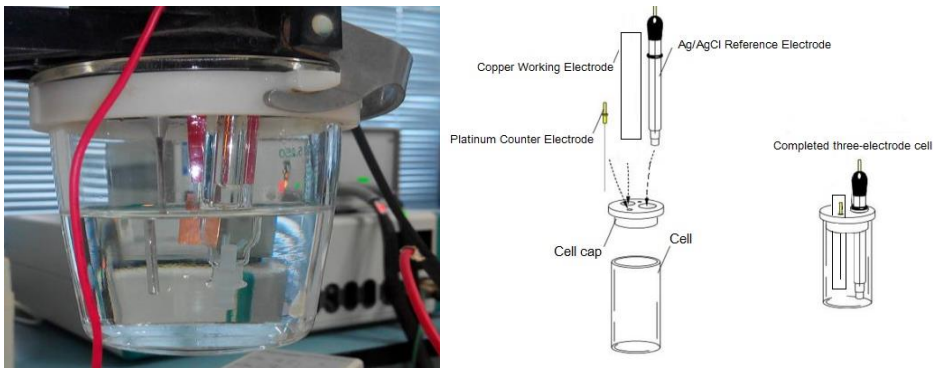

(a) (b)

Figure 2-1 A schematic of the three-electrode cell used for electrochemical measurements

2.4 Electrode preparation

2.4.1 Electrochemical measurements

For potentiodynamic polarization and EIS copper was mechanically polished with emery paper (#1000) and then degreased with acetone, dried at room temperature and then immersed immediately in the test solution. No attempt was made to remove the air-formed oxide film which may have formed on the metal surface prior to immersion. In the case of CV, GCE was polished with alumina (0.05 μm) water slurry on polishing cloth, rinsed well with distilled water and wiped several times with wetted soft tissue.

2.5 Sample preparation

2.5.1 Electrochemical measurements

For potentiodynamic polarization and EIS, appropriate amount of inhibitors were dissolved and their volume made up with acetonitrile. In the case of supporting electrolyte for CV, 0.3880 g of $TBAPF_6$ was dissolved in acetonitrile and the volume was made up to 100 mL. 1.0×10^{-3} M $CuCl_2$ was prepared by dissolving 0.0170 g of $CuCl_2 \cdot 2H_2O$ and its volume was made up to 100 mL with 0.0100 M $TBAPF_6$ in acetonitrile. Dimedone 0.0140 g was dissolved in acetonitrile and diluted to 100 mL to obtain 1.0×10^{-3} M solution. The mixture of copper (II) and dimedone solution was prepared by adding 0.0085 g of $CuCl_2 \cdot 2H_2O$ in 50 mL 1.0×10^{-3} M dimedone with 0.0100 M $TBAPF_6$ in acetonitrile.

2.5.2 Spectroscopic measurements

For UV-Vis spectroscopy, 1.0×10^{-3} M $CuCl_2$ was prepared by weighing 0.0170 g of $CuCl_2 \cdot 2H_2O$ and dissolved in acetonitrile and the volume was made up to 100 mL. Dimedone 0.0140 g was prepared in the same way to obtain the concentration of 1.0×10^{-3} M.

For FTIR, copper-dimedone complex solution was prepared by weighing 0.2800 g of dimedone (2.0×10^{-3} mol) and dissolved in 20.0 mL of methanol. $CuCl_2 \cdot 2H_2O$ 0.1705 g (1.0×10^{-3} mol) in 15 mL of methanol was added and

the solution was refluxed at 70 ^{o}C for 5 hours. After filtering, the filtrate was left at room temperature for 1 month to obtain green crystals. Which were further isolated by suction filtration, washed with acetone and dried in a vacuum desiccator. The sample obtained was ground to reduce the particle size to less than 5 mm in diameter. A small amount of powder sample (about 0.1-2% of the KBr amount, or just enough to cover the tip of spatula) was mixed with the KBr powder, subsequently ground for 3-5 min and then pressed to form a thin and transparent pellet.

2.6 Procedure

2.6.1 Electrochemical measurements

In polarization measurement, 50 mL of the test solution was pipetted into the 100 mL cell. The measurements were made after allowing the electrode to achieve the steady state potential under open-circuit condition at room temperature. The nature of inhibitor was interpreted via polarization curves with a potential from -0.5 to -0.05 V and scan rate of 0.5 mV/s on freshly-prepared copper electrodes. Inhibition efficiencies were then evaluated (*vide infra*) from corrosion current densities (j_{corr}) obtained by Tafel extrapolation method.

Impedance measurement was carried out in the same way as polarization measurement. Impedance spectra were obtained in the frequency range of 150 kHz to 0.1 Hz with perturbation amplitude of 10 mV. Inhibition efficiencies were evaluated from charge transfer resistance (R_{ct}) obtained by the Nyquist plot.

CV studies were carried out in a glass cell with a capacity of 100 ml. 50 mL mixture of copper (II) and dimedone solution was pipetted into the cell and cyclic voltammograms were recorded in the potential range of -1.800 to 1.800 V with scan rate of 100 mV/s.

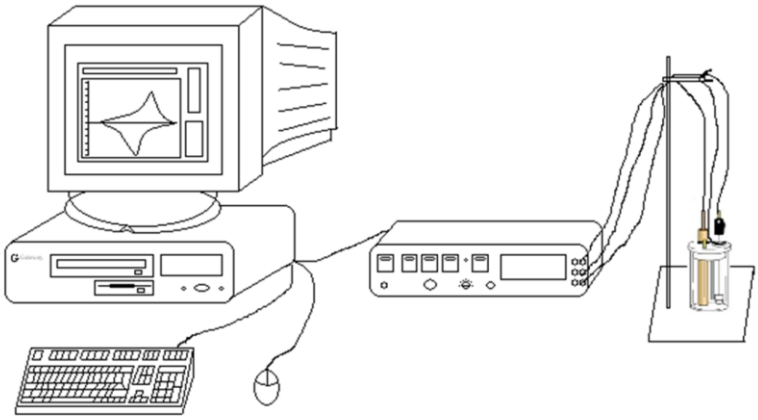

Figure 2-2 A schematic of the experimental setup used to record all electrochemical measurements (Ursula, 2013)

2.6.2 Spectroscopic measurements

UV-Vis spectroscopy

In the mole ratio method, different aliquots of 1.0×10^{-3} M dimedone solution as shown in Table 2-1 were added in 3.0 mL of 1.0×10^{-3} M copper (II) solution in order to get various metal ligand ratios ranging from 1:0.8 to 1:4.0. The absorbance was recorded at 246 nm and temperature maintained at 25℃.

Table 2-1 Volume of copper (II) and dimedone in the mole-ratio method

Ratio Copper (II) : Dimedone	**Volume (mL)**	
	Copper (II) 1.0x10^{-3} M	**Dimedone 1.0x10^{-3} M**
1.0 : 0.8	3.00	2.40
1.0 : 0.9	3.00	2.70
1.0 : 1.0	3.00	3.00
1.0 : 2.0	3.00	6.00
1.0 : 3.0	3.00	9.00
1.0 : 4.0	3.00	12.00

FTIR

The chemical structure of the sample was determined by using absorption FTIR spectroscopy at a resolution of 4 cm^{-1}. 16 additive scans were carried out between 4000 to 400 cm^{-1}.

2.6.3 Microscopy by SEM

After preparation, 1.0 × 1.0 cm^2 copper electrodes were immersed in the test solution for 6 h, dried at room temperature and then investigated by SEM.

2.6.4 Quantum chemical calculations

The structure of dimedone was drawn using GaussView program after that the geometry of the molecule was optimized by clicking on Clean up option. The optimized molecule file was input to calculate values of the highest occupied molecular orbital (E_{HOMO}), lowest unoccupied molecular orbital (E_{LUMO}), dipole moment (D) and Mulliken atomic charge distribution by clicking on: Calculate > Gaussian > Job Type > Energy > Method (RB3LYP DFT) > Basis Set (6-31G (d, p)) > Submit job. When Gaussian is finished running, a massage will be appeared on the screen.

CHAPTER 3

RESULTS AND DISCUSSION

3.1 Corrosion inhibition of copper by thiourea and N, O, S-ligating ring compounds

According to the preceding X-Ray crystallographic and cyclic voltammetric studies on the complexation of copper (I) halides and substituted thiourea (Chuaysong et al., 2008), the obtained results can be used for describing corrosion inhibition abilities of thiourea and substituted thiourea under the conditions as shown in Table 3-1.

3.1.1 Corrosion inhibition of copper by thioureas

With the results from corrosion investigation of copper in four types of ureas namely thiourea (tu), diphenylthiourea (dptu), phenylthiourea (ptu) and ethylene thiourea (etu) in acetonitrile as shown in Table 3-1 it was found that copper corrodes to the greatest extent in dptu with the corrosion inhibition of 98.98% and etu is the best inhibitor in this group (99.48%), %*IE* are calculated from equation *(19)*. This is due to the fact that, in term of inductive effect, ethylene is electron releasing group hence the enhancement of its capability in forming the substances covering the surface. In contrast, phenyl group, despite its similar inductive effect as an electron donor, its steric structure hurdles the proximity to surface to undergo redox reactions to form the substances to cover the surface and inhibit copper corrosion at this concentration. It has already been shown that at lower concentration (‹ 0.1 M) tu exhibits corrosion inhibiting characteristics in contrast to the case of high corrosion of which Cu-tu can form well and strip off the surface easily (Zhao and Cui, 2011). Furthermore, both structure and substitutent groups have been proved to affect the corrosion behavior (Mostafa et al., 2002). In the case of Pd, the phenyl group was shown to have planar structure (Anderson et al., 2010) which makes it much more difficult to reach the metal surface. All of the contributors discussed above lead to the order of corrosion inhibition of etu > tu > ptu > dptu.

Table 3-1 Corrosion inhibition by thioureas in acetonitrile

Entry	**Thiourea Type (1 mM)**	**Additional substance**	j_{corr}/**A cm^{-2}**	***IE%* ± SD**
1	Thiourea	-	2.97×10^{-8}	99.22 ± 0.04
2	Diphenyl Thiourea	-	3.89×10^{-8}	98.98 ± 0.04
3	Phenyl Thiourea	-	3.26×10^{-8}	99.14 ± 0.02
4	Ethylene Thiourea	-	1.96×10^{-8}	99.48 ± 0.03
5	Thiourea	1 mM Cl^-	1.10×10^{-5}	-187.44 ± 0.68
6		1 mM I^-	4.67×10^{-5}	-1126.73 ± 0.98
7		1 mM Br^-	2.32×10^{-5}	-510.35 ± 0.72
8	Diphenyl Thiourea	1 mM Cl^-	2.66×10^{-6}	30.21 ± 0.85
9		1 mM I^-	3.95×10^{-5}	-936.61 ± 0.35
10		1 mM Br^-	2.40×10^{-5}	-526.96 ± 0.24
11	Phenyl Thiourea	1 mM Cl^-	1.02×10^{-5}	-168.58 ± 0.47
12		1 mM I^-	4.65×10^{-5}	-1119.94 ± 0.26
13		1 mM Br^-	3.96×10^{-5}	-940.38 ± 0.23
14	Ethylene Thiourea	1 mM Cl^-	1.06×10^{-5}	-178.39 ± 0.45
15		1 mM I^-	4.65×10^{-5}	-1119.94 ± 0.25
16		1 mM Br^-	1.26×10^{-5}	-232.18 ± 0.75
17	-	-	3.81×10^{-6}	0.000 ± 0.40

When halides are added in the solution, it is usual that copper corrosion increases because of the formation of stripping complex speculated to be $CuCl_2^-$ (Finsgar and Merl, 2014). With the comparison of the three halides, it was found that all four types of thioureas exhibit the same trend of iodide > bromide > chloride, corresponding with electrochemical and X-ray Crystallography results for copper (I) complexes (Singhagomol, 1999 and Chuaysong et al., 2008) which reveal that, for copper dptu-halide complexes, iodide has with the longest bond distance and only acts as a charge balancing ion hence its has greater freedom to form copper-halide complex and increase the corrosion of copper directly via complex formation

whereas bromide and chloride ions can bond with copper strongly and cause less electron density as well as reduce the extent of corrosion due to the fact that it cannot attack the metal surface directly in the same way as free ions.

Another interesting point is that, with the same halide, the corrosion inhibition trend for Cl^- and I^- is that dptu < ptu < etu < tu. This is due to the fact that the structure of $Cu(dptu)_2^+$ is trigonal planar (Singhagomol, 1999) which facilitates the absorption of thiourea ligand on copper metal. In the case of tu, the structure is tetrahedral which is more steric than trigonal planar with the trend to include another additional tu ligand (Okaya and Knobler, 1964). Ligands ptu and etu has similar coordination number to dptu, but the complexes have similar trend to become dimer (Battaglia et al., 1976 and Bowmaker et al., 2009), causing copper corrosion rate to be essentially the same. For Br^-, two doubly bridging etu (Bowmaker et al., 2009) seems to influence greater adsorption on copper at low concentration and causes different trend (etu < tu < dptu < ptu) from those of Cl^- and I^-. These results represent the close and subtle relationship between the structure of complex on adsorption on the surface and, in turn, corrosion inhibition characteristics.

3.1.2 Corrosion inhibition by N, O, S-ligating ring compounds

In contrast to thioureas, N, O, S-ligating ring compounds seem to form complex with copper and attach to the surface since our results reveal that the order of capabilities of corrosion inhibition is nitrogen > oxygen > sulfur > carbonyl, reflecting greater affinity for nitrogen in forming complex with copper as a film on copper surface (Milan et al., 2009). Acridone therefore exhibits the greatest corrosion inhibition with the corrosion inhibition of 98.98%. In the case of oxygen, and the presence of carbonyl group has no effect on corrosion rate (Entry 1 and 2 of Table 3-2).

Table 3-2 Corrosion inhibition by N, O, S-ligating ring compounds (O* = carbonyl)

Entry	Ligating Ring Compounds Type (1 mM)	Ligating atom	Additional substance	j_{corr}/A cm^{-2}	*IE%* ± SD
1	Xanthone	O, O*	-	9.04×10^{-8}	97.62 ± 0.04
2	Xanthene	O	-	8.64×10^{-8}	97.73 ± 0.05
3	Thioxanthone	S, O*	-	1.14×10^{-7}	97.00 ± 0.03
4	Acridone	N, O*	-	3.87×10^{-8}	98.98 ± 0.01
5	1,4-naphthoquinone	2O*	-	2.74×10^{-7}	92.85 ± 0.03
6	1,4-naphthoquinone	2O*	0.1 M Aniline	5.78×10^{-7}	84.82 ± 0.43
7	1,4-naphthoquinone	2O*	0.1 M Acetic acid	2.22×10^{-6}	41.72 ± 0.31
8	-	-	-	3.81×10^{-6}	0.000 ± 0.40

When there is no free ligating atom of N, O and S such as in the case of 1,4-naphthoquinone, weak interaction between carbonyl group and copper results in greater corrosion. Furthermore, the corrosion rate in acidic conditions is higher than that in the basic ones, which is normally the case for acid sensitive metal like copper (Sudheer and Quraishi, 2013).

3.2 Corrosion inhibition of copper by dimedone

Dimedone is a quinone compound used in organic chemistry to investigate whether a compound contains an aldehyde group. It can also be used as catalyts in the formation of transition-metal complexes. Due to the fact that the mechanism of corrosion inhibition by dimedone has not been elucidated comprehensively, thus corrosion inhibition behaviours of dimedone is next the topic to be focused.

3.2.1 Potentiodynamic polarization

Figure 3-1 illustrates the potentiodynamic polarization curves of copper in acetonitrile with and without dimedone from which relevant parameters are

obtained (Table 3-3) namely corrosion potential (E_{corr}), corrosion current density (j_{corr}), cathodic and anodic Tafel slopes (β_c, β_a) and corrosion inhibition efficiency (*IE%*).

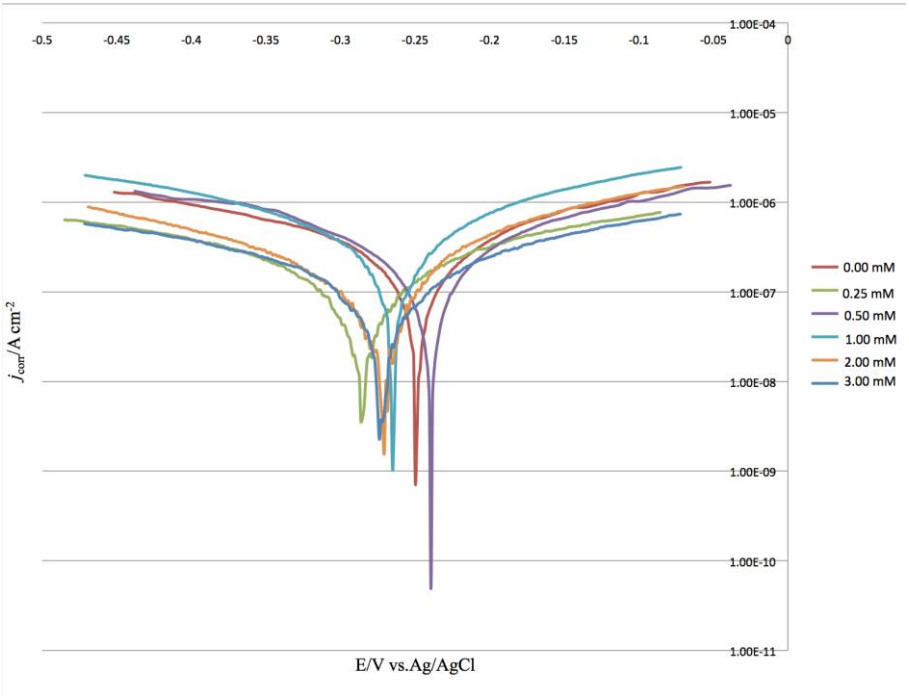

Figure 3-1 Potentiodynamic polarization curves for copper in acetonitrile at room temperature in absence and presence dimedone at various concentrations

The presence of dimedone causes small fluctuations of E_{corr} between -0.24 V and -0.30 V, indicating that dimedone acts as a mixed-type corrosion inhibitor which suppresses both anodic and cathodic reaction simultaneously (Amin and Khaled, 2010). This suppression of the corrosion process possibly results from adsorbed of dimedone molecules on copper surface which blocks corrosion mechanism. It is clear that j_{corr} greatly decreases from 3.81×10^{-6} to 0.44×10^{-6} Acm^{-2} with the presence of the dimedone and the *IE%* calculated from j_{corr} increases with dimedone concentration, with the concentration over 3.00 mM, *%IE* was only slightly increased which was possibly due to surface saturation.

Table 3-3 Polarization parameters of copper in acetonitrile solution in absence and presence of dimedone at different concentrations at room temperature

$C_{dimedone}$ mM	β_a (V decade^{-1})	β_c (V decade^{-1})	j_{corr} (A cm^{-2})	E_{corr} (V vs Ag/AgCl)	*IE%* ± SD
0.00	31.55	1.28	3.81×10^{-6}	-0.25	0.000 ± 0.40
0.25	7.12	2.06	2.47×10^{-6}	-0.29	35.17 ± 0.40
0.50	1.84	1.34	2.44×10^{-6}	-0.24	35.95 ± 0.66
1.00	0.90	0.56	1.56×10^{-6}	-0.27	59.06 ± 0.66
2.00	0.76	0.36	0.52×10^{-6}	-0.27	86.48 ± 0.04
3.00	0.30	0.22	0.44×10^{-6}	-0.30	88.37 ± 0.03

3.2.2 Electrochemical impedance spectroscopy (EIS)

The influence of dimedone on the adsorption process and corrosion inhibition on copper surface can be partially obtained by EIS. The Nyquist diagram for copper in acetonitrile solution, without and in the presence of different concentrations of dimedone, were similar in shape (Figure 3-2) of a single semicircle which indicates the corrosion reaction is controlled by the charge transfer process (Yurt et al., 2004; Zhang and Hua, 2009 and Deyab, 2015).

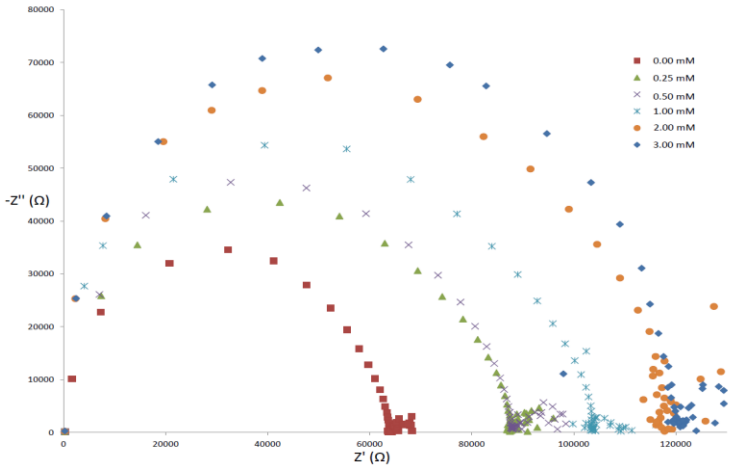

Figure 3-2 Nyquist plots copper in acetonitrile solution containing various concentrations of dimedone at room temperature

With the analysis of impedance data using the equivalent circuit (EC) as shown in Figure 3-3, charge transfer resistance (R_{ct}) and double-layer capacitance (C_{dl}) were obtained (Table 3-4).

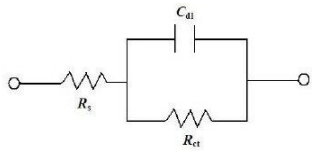

Figure 3-3 Equivalent circuit (EC) model used to fit the experimental impedance data. In which R_s represent the solution resistance, R_{ct} charge transfer resistance *Cdl* are constant phase elements for double layer

It is apparent that the (R_{ct}) values of copper in acetonitrile solution significantly increased with increasing amount of dimedone, indicating that the presence of dimedone improved copper corrosion inhibition. Additionally, the decrease in C_{dl} values caused both the decrease in the dielectric constant and the increase of the double layer thickness, also supporting the adsorption of dimedone on the copper/solution interface (Naqvi et al., 2011). Finally, progressive covering of copper surface by dimedone leads to the maximum inhibition efficiency of 93.68% with dimedone at the 3.0 mM (Table 3-4), %*IE* are calculated from equation *(26)*. *%IE* values obtained from EIS are in good agreement with those obtained by potentiodymic polarization measurement (t-test, $P < 0.05$)

Table 3-4 Electrochemical impedance parameters for copper in acetonitrile solution in the absence and presence of inhibitor at different concentrations at room temperature

$C_{dimedone}$ (mM)	R_s (Ω cm^2)	R_{ct} (Ω cm^2)	C_{dl} (F)	*IE%* ± SD
0.00	257.60	63.71×10^{-3}	7.24×10^{-11}	0.000 ± 0.02
0.25	262.10	88.18×10^{-3}	4.15×10^{-11}	38.41 ± 0.02
0.50	245.62	88.74×10^{-3}	3.80×10^{-11}	39.29 ± 0.02
1.00	258.00	104.54×10^{-3}	2.80×10^{-11}	64.09 ± 0.01
2.00	250.32	117.84×10^{-3}	2.00×10^{-11}	84.95 ± 0.01
3.00	261.49	123.40×10^{-3}	1.78×10^{-11}	93.68 ± 0.01

3.2.3 Adsorption isotherm

The adsorption isotherm is an effective way to explain the adsorption mechanism of the inhibitors (Musa et al., 2010). A number of adsorption isotherms were tested for dimedone adsorption on copper, including Freundlich, Temkin and Langmuir isotherms. Langmuir isotherm (equation *(31)*) was found to provide the best description for the adsorption behaviour of dimedone (Table 3-5).

Table 3-5 The correlation coefficient (R^2) values for adsorption of dimedone on copper surface obtained from Langmuir, Freundlich, and Temkin adsorption isotherms

Adsorption Isotherms	**Potentiodynamic Polarization**	**EIS**
	R^2	R^2
Langmuir	0.9652	0.9780
Freundlich	0.9325	0.9427
Temkin	0.9269	0.9451

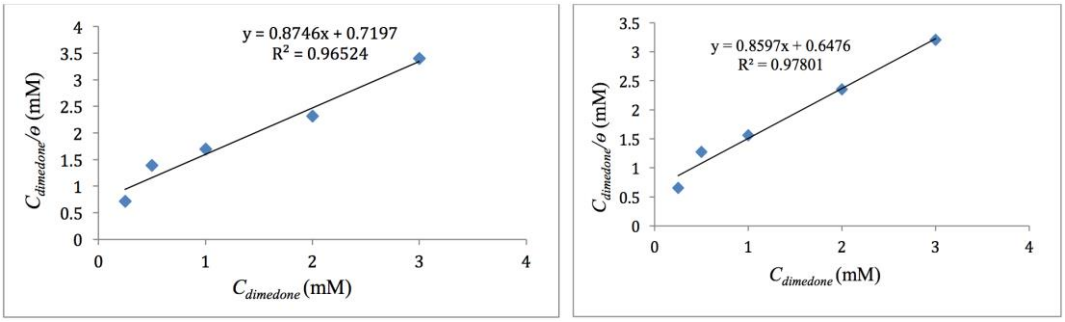

(a) (b)

Figure 3-4 Langmuir adsorption isotherm by polarization (a) and (b) EIS measurement of dimedone on copper surface in acetonitrile at room temperature

The surface coverage degree θ was calculated by *IE%*/100 (Deyab, 2015) from both impedance and polarization measurements with good agreement of linear relationships between $C_{dimedone}/\theta$ and $C_{dimedone}$ (Figure 3-4). Linear correlation coefficients (R^2) of 0.9652 and 0.9780 from potentiodynamic polarization and EIS techniques respectively, indicating that the adsorption of dimedone on copper surface at 298 K obeys the Langmuir adsorption isotherm (Sudheer and Quraishi, 2013).

Table 3-6 Adsorption parameters on copper corrosion inhibition by dimedone in acetonitrile at 298 K obtained from Langmuir isotherm

Techniques	**Intercept (mM)**	**K_{ads} (mM)**	**ΔG^o_{ads} (kJmol^{-1})**
Potentiodynamic polarization	0.72	1.39	-8.43
EIS	0.65	1.54	-8.17

K_{ads} can then be calculated from the intercepts to be 1.39 and 1.54 mM from potentiodynamic polarization and EIS respectively (Table 3-6). K_{ads} is related to standard energy of adsorption (ΔG^o_{ads}) by the equation *(34)*. Calculated ΔG^o_{ads} from impedance and polarization data was -8.43 and -8.17 kJmol^{-1} respectively. ΔG^o_{ads} of -20 kJmol^{-1} or lower indicates physisorption whereas that about -40 kJ mol^{-1} involves

charge sharing or a transfer from the inhibitor molecules to the metal surface to form a coordinate type of bond (chemisorption) (Hegazy et al., 2015). Hence the adsorption of dimedone compounds is of physisorption type. The negative values of ΔG^{o}_{ads} reveals the spontaneity of adsorption process and stability of the adsorbed layer on the copper surface.

3.2.4 Cyclic voltammetry

The redox behavior of copper (II) in copper (II) chloride in 0.0100 M $TBAPF_6$ in acetonitrile by cyclic voltammetry on glassy carbon electrode at room temperature confirms the formation of copper (II) dimedone complex (Fig 3-5).

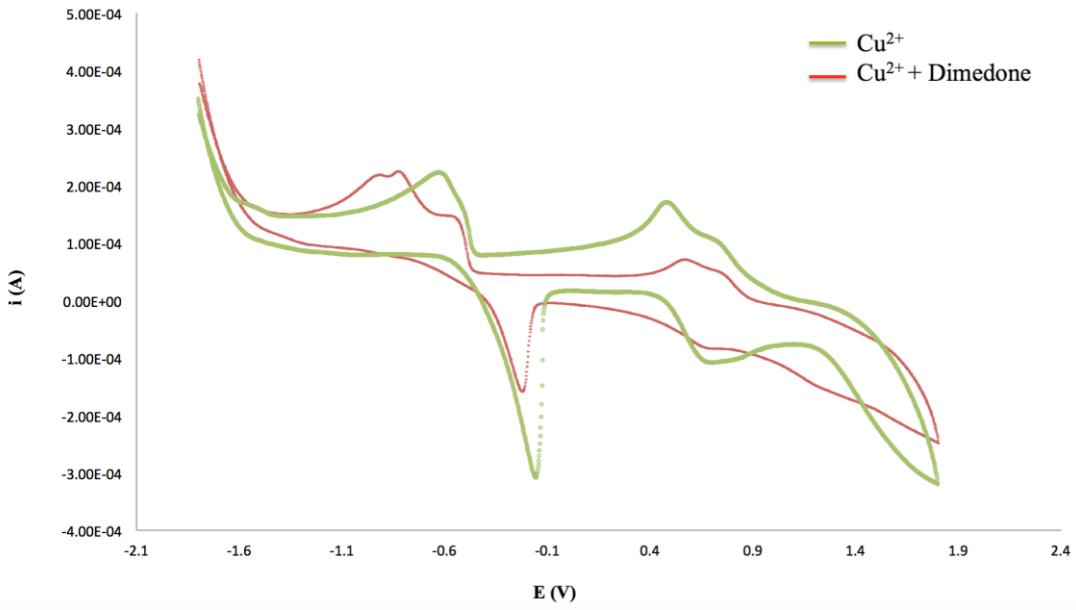

Figure 3-5 Cyclic Voltammogram of 1.00 mM of $CuCl_2.2H_2O$ at -1.800 – 1.800 V potential window and 100 mVs^{-1} scan rate in the presence of 0.0100 M $TBAPF_6$ as supporting electrolyte in acetonitrile

The shift of both reduction peaks of copper (II) to more negative reveals less electron density which makes accepting electron more difficult. On the other hands, oxidation peaks shift to more positive which also indicates less possibilities in transferring electron due to complex formation. Similar behaviors are

found for the case of peaks from dimedone, especially oxidation. The complexation ratio of copper-dimedone was also found to be 1:2 by mole ratio method (Fig 3-6).

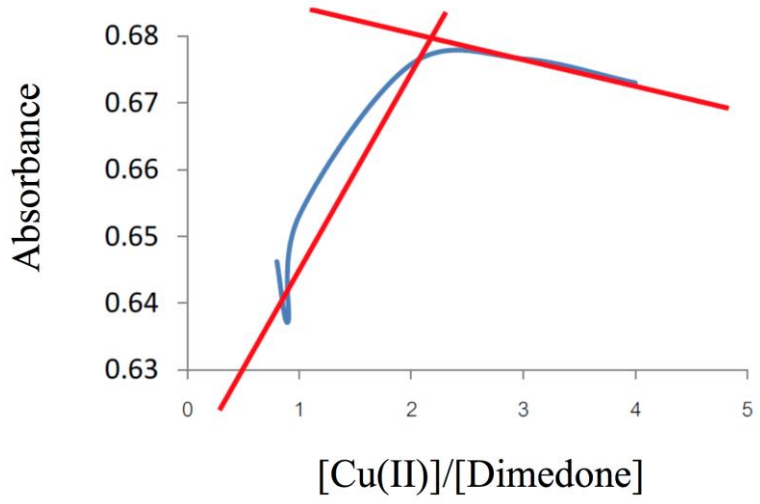

Figure 3-6 Mole ratio of $CuCl_2 \cdot 2H_2O$ with dimedone (λmax = 246 nm) in acetonitrile solution

3.2.5 Fourier transform infrared spectroscopy (FT-IR)

Figure 3-7 shows FT-IR spectrum of solid dimedone on KBr pellet. The spectrum shows a peak bands of C-H stretching at 2956.09 cm^{-1}, C=O stretching at 1733.82 cm^{-1} and C-H bending at 1411.74 cm^{-1}. The same characteristic bands appeared for copper (II) dimedone complex with strong C=O stretching modification (Figure 3-8 and Table 3-7): the bands of C=O stretching had disappeared due to the formation of stable O-Cu bond (Rajkumar and Sethuraman, 2014), C-H stretching at 2961.00 cm^{-1} and C-H bending at 1421.66 cm^{-1} (Yadav et al., 2013). The shift indicates the change of electron cloud density due to the coordination with copper (II) (Kalsi, 2008).

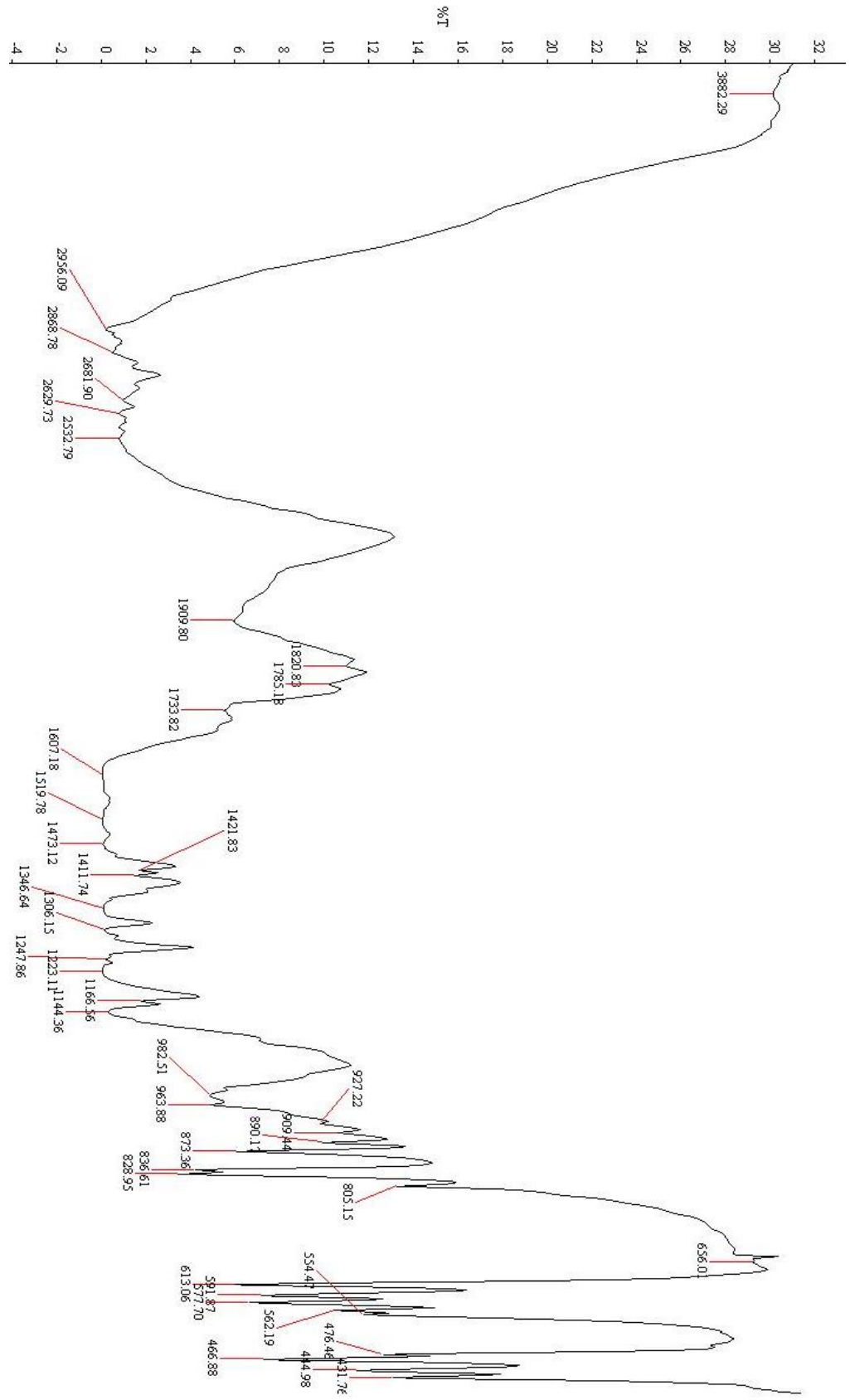

Figure 3-7 IR spectrum of Dimedone

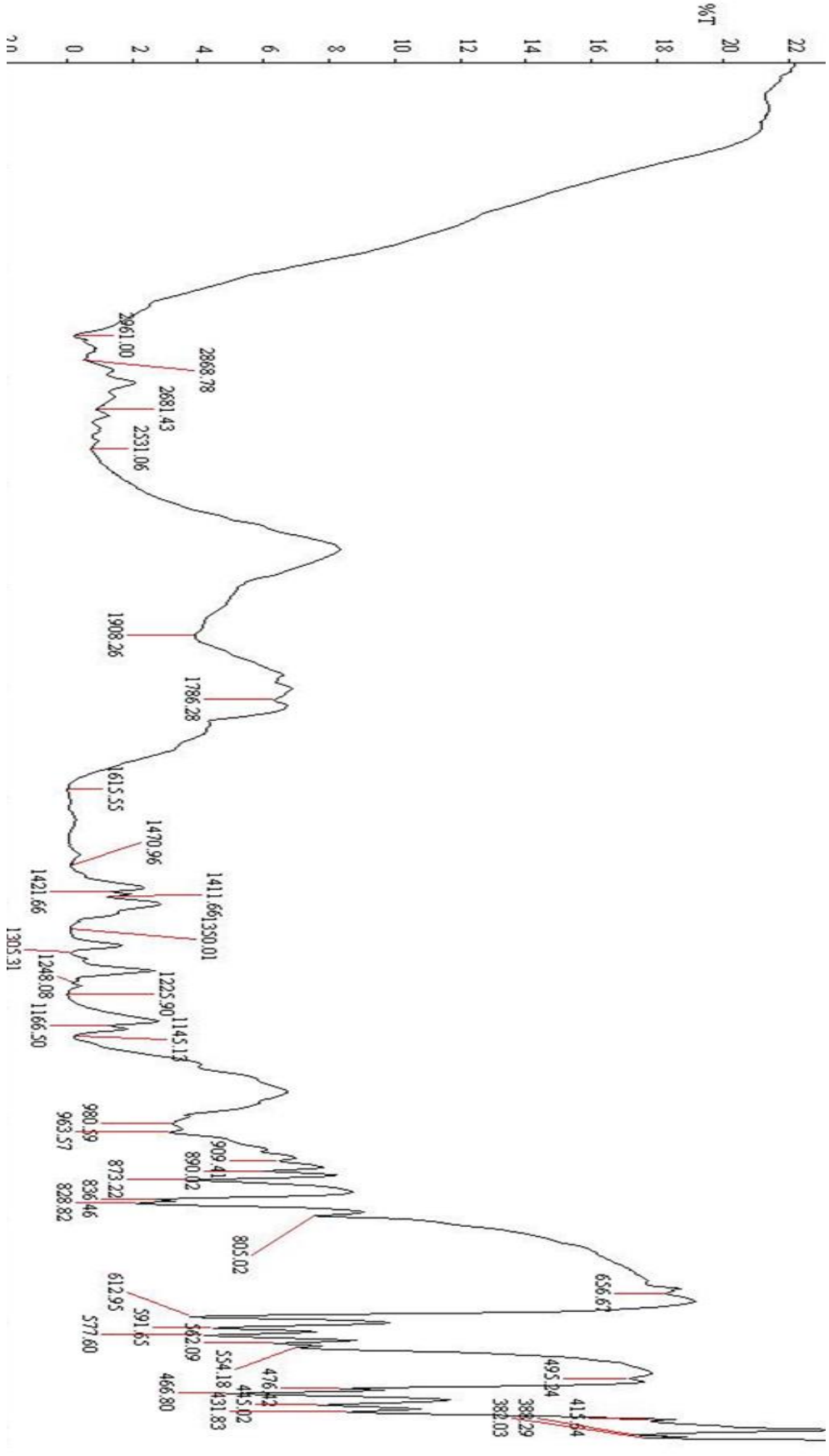

Figure 3-8 IR spectrum of Dimedone and $CuCl_2 \cdot 2H_2O$

Table 3-7 Frequencies of the bands in the IR spectra of dimedone and dimedone-$CuCl_2$ complex

Remarkable functional groups	**Dimedone**	**Dimedone with $CuCl_2 \cdot 2H_2O$**
C-H stretching	2956.09 cm^{-1}	2961.00 cm^{-1}
C=O stretching	1733.82 cm^{-1}	disappear
C-H bending	1411.74 cm^{-1}	1421.66 cm^{-1}

3.2.6 Morphological studies of copper surface

Copper surface was characterized by SEM whose results without dimedone shown in Figure 3-9 (a) indicate smooth surface with certain scratches on the bare copper surface caused by polishing in the electrode cleaning process. With dimedone, a protective layer is shown (Figure 3-9 (b)) in good accordance with the results obtained from potentiodynamic measurements and EIS.

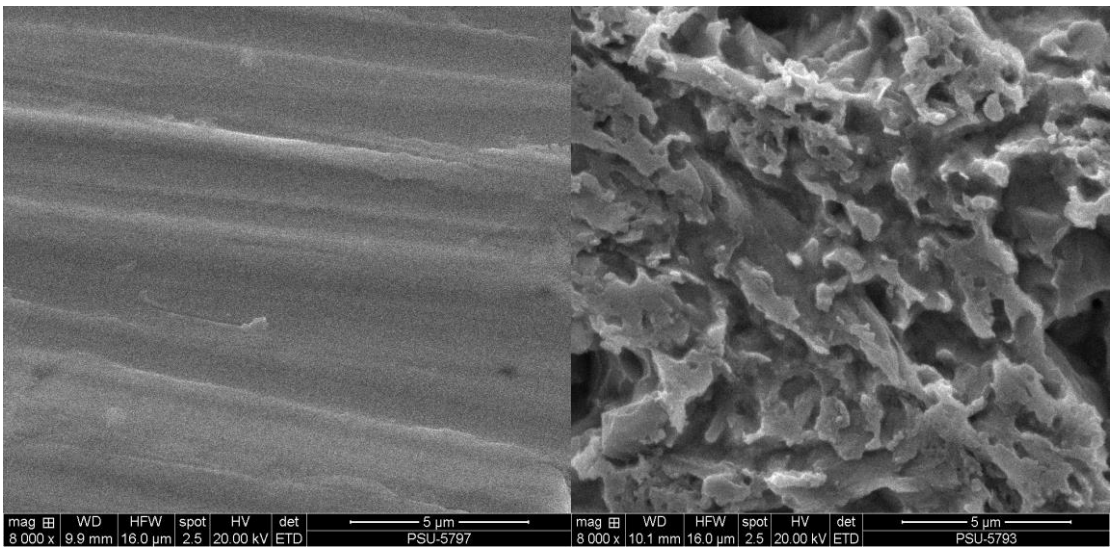

(a) (b)

Figure 3-9 SEM micrographs of (a) bare copper surface and (b) copper surface (at 8,000 magnification) in the presence of 3.00 mM dimedone after 6 h

3.2.7 Quantum chemical calculations

To investigate the effect of molecular structure on inhibition mechanism, quantum chemical calculations were performed for neutral species. The geometry of dimedone compound was determined by optimizing all geometrical variables without any symmetry constraints to obtain the result shown in Figure 3-10(c). Certain quantum chemical parameters are related to the interactions between the inhibitor and the copper surface including E_{HOMO}, E_{LOMO} and dipole moment (D). E_{HOMO} is associated with the capacity of a molecule to donate electrons and the increase in the value of E_{HOMO} can facilitate adsorption hence the inhibition efficiency, which also indicates the disposition of the molecule to donate orbital electrons to an appropriate acceptor with empty molecular orbitals (Ahmed et al., 2012). In contrast, E_{LUMO} indicates the ability of the molecule to accept electrons. The lower the value of E_{LUMO}, the more probable is the molecule to accept electrons. Low absolute value of the energy band gap (E_{HOMO} - E_{LUMO}) renders good inhibition efficiencies because it means lower energy to remove an electron from the highest occupied orbital (Ahmed et al., 2012). Dimedone was found to have high HOMO (-0.2449 hartree) (Table 3-8) with the preferred active sites for an electronic attack and the favourite sites for interaction with the metal surface located at 1,3-cyclohexanedione in the molecule (Figure 3-10 (a)) whereas its E_{LUMO} is low (-0.0358 hartree). Additionally low energy gap of 0.2091 hartree support dimedone high inhibitory performance. The dipole moment of the molecule is also calculated due to the fact that it is influenced by the molecular structure and is expected to play a role in the adsorption process (Ahmed et al., 2012). High D of dimedone (3.6935, Table 3-8) reveals the favor of the molecule to accumulate on the surface layer and in turn reduce the rate of electrochemical reaction (Raafat et al., 2008).

Table 3-8 Quantum chemical parameters of dimedone

Inhibitor	E_{HOMO}(hartree)	E_{LUMO}(hartree)	ΔE (hartree)	Dipole Moment(D)
Dimedone	-0.2449	-0.0358	0.2091	3.6935

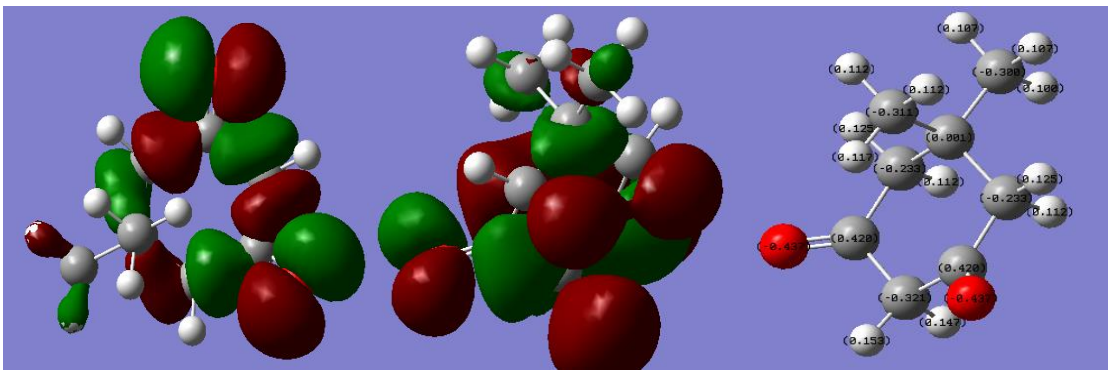

(a) (b) (c)

Figure 3-10 (a) E_{HOMO}, (b) E_{LUMO}, and (c) Mulliken atomic charge distribution of dimedone molecule calculated by RB3LYP DFT method

The Mulliken atomic charge distribution calculated using the RB3LYP DFT method is presented in Fig 3-10 (c). Oxygen and some carbon atoms have higher charge densities so they are generally the sites where electrophiles attack. Therefore, O and C atoms were active centers with the ability to form a protective film by physical adsorption with copper surface. In addition, the HOMO (Fig. 3-10 (a)) was mainly distributed on 1,3-cyclohexanedione, the framework of dimedone, which therefore probably the primary site in forming a protective film.

It could be deduced on the above discussion that dimedone, apart from existing in the anionic form which can interact with copper surface by electrostatic attraction, may also interact with the copper surface via oxygen and carbon atoms, forming an effective protective layer on the copper surface thus retarding further corrosion of the metal in acetonitrile. The efforts are currently put for synthesizing crystals suitable for x-ray crystallography to further support our results.

CHAPTER 4

CONCLUSION

Corrosion is the primary cause of serious engineering problems and of great economic concern. It has a number of effects on the safe and efficient operation of equipment as well as durability of structure. It is clear that the best way to combat corrosion is protection. Various prevention methods are used to prevent degradation of metal surface, the corrosion inhibitor is the one of the most useful method that has been used for many decades on industry due to excellent anti-corrosive, low cost and practice method. Inorganic inhibitors such as chromate, phosphate, molybdate, and nitrites are generally accepted as efficient corrosion inhibitor that can protect metals by forming a protective barrier film. However, the use of inorganic inhibitors are becoming increasing restrictive because of their high degree of toxicity. Consequently, this has given incentive to search for less toxic inhibitors. Currently, organic inhibitors are being extensively used as an alternative to replace inorganic inhibitors. The corrosion inhibition efficiency of organic corrosion inhibitors is related to the present of polar functional groups in their molecules as well as pi electrons in heterocyclic ring which can strongly adsorb on the metal surface to form a protective film and provide a barrier to dissolution of the metal in the electrolyte. This research presents the corrosion inhibition of copper by two groups of organic inhibitors including thioureas and quinones in acetonitrile.

For thioureas, copper exhibits quite similar corrosion rate with the lowest in the case of ethylene thiourea compared with phenylthiourea due to the least steric effect. With the presence of halides, iodide causes greatest corrosion due to its freedom to attack copper surface, in good agreement with the result by X-ray Crystallography and electrochemistry. Trigonal planar structure and bridging ligands facilitates the bonding and corrosion inhibition whereas dimer formation cause adverse effect.

In the case of N, O, S-ligating ring compounds, the formation of bonds between copper and can inhibit corrosion with the capability in the order of nitrogen >

oxygen > sulfur > no ligating atoms.

Inhibition efficiency of dimedone towards copper corrosion in acetonitrile solution was determined by electrochemical techniques including polarization and impedance measurements to obtain 88.37 and 93.68% respectively. Potentiodynamic polarization revealed that dimedone is a mixed-type corrosion inhibitor of which efficiency increases with concentration with high inhibition efficiency. Protection afforded by dimedone is due to its physical adsorption obeying Langmuir isotherm. The adsorption layers and corresponding complexes formed by dimedone are further confirmed by the results from CV, SEM, UV-Vis and FTIR analysis. From calculated standard energy of adsorption and quantum chemical calculations, the driving force for the formation of protective film could be the physisorption via the oxygen and carbon atoms.

REFERENCES

Ahmed, Y.M., Abu, B.M., Mohd, S.T., and Ramzi, T.T.J. 2012. Electrochemical and quantum chemical studies on phthalhydrazide as corrosion inhibitor for mild steel in 1 M HCl solution. *Res Chem Intermed* **38,** 453–461.

Amin, M.A., and Khaled, K.F. 2010 Copper corrosion inhibition in O_2-saturated H_2SO_4 solutions. *Corrosion Science* **52,** 1194–1204.

Anees, A. 2008 Adsorption isotherm of some triazoles as corrosion inhibitors of mild steel in acids. AL-Fatih **32**, 1-10.

Anees, A.K., Ahmed, F.H., and Baker, M.A. 2015. Evaluation of environmentally friendly inhibitor for galvanic corrosion of steel–copper couple in petroleum waste water. *Process Safety and Environmental Protection* **98,** 93–101.

Bard, A.J., and Faulkner, L.R. 2000. *Electrochemical Methods: Fundamentals and Applications.* 2 nd Edition, John Wiley & Sons. New York.

Barouni, K., Kassale, A., Bazzi, L., Salghi, R., Hammouti, B., Albourine, A., Issami, S. El., Jbara, O., and Bouachrine, M. 2014. Inhibition of corrosion of copper in nitric acid solution by four amino acids. *Research on Chemical Intermediates* 40, 991–1002.

Behpour, M., and Mohammadi, N. 2012. Investigation of inhibition properties of aromatic thiol self-assembled monolayer for corrosion protection. *Corrosion Science* **65,** 331–339.

Behpour, M., and Mohammadi, N. 2013. Use of Compounds Containing Heteroatoms as Electrochemical Corrosion Inhibitors for Copper in Hydrochloric Acid. *Chemical Engineering Communications* **200,** 351-366.

Bhawsar, J., Jain, P. K, and Jain, P. 2015. Experimental and computational studies of

Nicotiana tabacum leaves extract as green corrosion inhibitor for mild steel in acidic medium. *Alexandria Engineering Journal*. **54,** 769-775.

Bowmaker, G. A., Pakawatchai, C., Skelton, B. W., Thanyasirikul, Y., and White, A. H. 2008. Structural and Spectroscopic Studies of $[M((x)tu)\ 4\ ]^{+}$ Systems (M = Cu, Ag; (x)tu = (substituted) Thiourea). *Zeitschrift für anorganische Chemie* **14,** 2583 – 2588.

Chen, W., Hong, S., Li H., Luo, H., Li, M., and Li, N. 2012. Protection of copper corrosion in 0.5 M NaCl solution by modification of 5-mercapto-3-phenyl-1,3,4-thiadiazole-2-thione potassium self-assembledmonolayer. *Corrosion Science* **61,** 53–62.

Chuaysong, R., Chooto, P., and Pakawatchai, C. 2008. Electrochemical properties of copper (I) halides and substituted thiourea complexes. *Science Asia* **34,** 440-442.

Cofre, P., and Bustos, A. 1994. Voltammetric behavior of the copper(II)-thiourea system in sulphuric acid medium at platinum and glassy carbon electrodes. *Journal of Applied Electrochemistry* **24,** 564-568.

Collins, A.M. 2012. Photo-electrochemical processes at the triple phase boundary. PhD Thesis, University of Bath.

Deyab, M.A. 2015. Hydroxyethyl cellulose as efficient organic inhibitor of zince carbon battery corrosion in ammonium chloride solution. Electrochemical and surface morphology studies. *Journal of Power Sources* **280,** 190-194.

Elmsellem. H., Basbas. N., Chetouani. A., Aouniti. A., Radi. S., Messali. M., and Hammaouti. B. 2014. Quantum chemical studies and corrosion inhibitive properties of mild steel by some pyridine derivatives in 1 M HCl solution. *Portugaliae Electrochimica Acta* **32,** 77-108.

El-Egamy, S.S. 2008. Corrosion and corrosion inhibition of Cu–20%Fe alloy in sodium chloride solution. *Corrosion Science* **50,** 928 – 937.

Foo, K.Y., and Hameed, B.H. 2010. Insights into the modeling of adsorption isotherm systems. *Chemical Engineering Journal* **156,** 2-10.

Gece, G. 2008. The use of quantum chemical methods in corrosion inhibitor studies. *Corrosion Science* **50,** 2981–2992.

Gil, P.M. 2013. Exploring corrosion inhibition in acid and oil field environments. PhD Thesis, The University of Manchester.

Gomez, H., Lizama, H., Suarez. C., and Valanzuela, A. 2009. Effect of thiourea concentration on the electrochemical behavior of gold and copper electrodes in presence and absence of Cu (II) ions. *Journal of the Chilean Chemical Society*. **54,** 439-444.

Hegazy, M.A., Nazeer, A.A., and Shalabi, K. 2015. Electrochemical studies on the inhibition behavior of copper corrosion in pickling acid using quarternary ammonium salts. *Journal of Molecular Liquids* **209,** 419–427.

Hong, S., Chen, W., and Li, N. 2012. Inhibition effect of 4-amino-antipyrine on the corrosion of copper in 3 wt.% NaCl solution. *Corrosion Science* **57,** 270–278.

Hong, S., Chen, W., Zhang, Y., Li, M., and Li, N. 2013. Investigation of the inhibition effect of trithiocyanuric acid on corrosion of copper in 3.0 wt.% NaCl. *Corrosion Science* **66,** 308–314.

http://serc.carleton.ed u/research_education/ geochemsheets/techniques/SEM. html, Dec. 22, 2014 (accessed 12/09/2016).

http://www.bath.ac.uk/-chsacf/solartron~electro/html/cv.htm. (accessed 10/11/2016).

http://www.mmrc.caltech.edu/FTIR/FTIRintro.pdf, 2001 (accessed 1/06/2017).

Jeyaprabha, C., Sathiyanarayanan, S., Phani, K. L.N., and Venkatachari, G. 2005. Influence of poly(aminoquinone) on corrosion inhibition of iron in acid media. *Applied Surface Science*. **252,** 966-975.

Jones, D.A. 1995 Principle and prevention of corrosion. 2 nd Edition, Prentice-Hall. London.

Kalsi, P. S. 2008. Spectroscopy of Organic Compounds 6 th Edition, New Age International. Pvt. Ltd. Publishers. New Delhi.

Kar, B. 2009. Study Of Mitigation of Corrosion Rate of Mild Steel using Green Inhibitors. PhD Thesis, Jadavpur University, India.

Kazeem, O., Sanusi, E.T., Esther, A., Muzenda, E., and Akinlabi, S.A. 2015. Enhancement of corrosion resistance behaviour of Frictional Stir Spot Welding of Copper. *Proceedings* **2,** 1157 – 1165.

Kaya, S., Burak Tüzün, B., Kaya, C., and Obot, I.B. 2015. Determination of corrosion inhibition effects of amino acids: Quantum chemical and molecular dynamic simulation study. *Journal of the Taiwan Institute of Chemical Engineers* **58,** 1–8.

Khaled, K.F. 2009. Experimental and atomistic simulation studies of corrosion inhibition of copper by a new benzotriazole derivative in acid medium. *Electrochimica Acta* **54,** 4345–4352.

Khadom, A.A. 2010. Mathematical and quantum chemical studies for the corrosion inhibition of steel In HCl acid. *Diyala Journal of Engineering Sciences* **03,** 107-122.

Khadom, A.A., Hassan A.F., and Abod, B.M. 2015. Evaluation of environmentally friendly inhibitor for galvanic corrosion of steel–copper couple in petroleum waste water. *Process Safety and Environmental Protection* **98,** 93–101.

Khan, P.F., Shanti, V., Babu, R.K., Muralidharan, S., and Barik, R. C. 2015. Effect of benzotriazole on corrosion inhibition of copper under flow conditions. *Journal of Environmental Chemical Engineering* **3,** 10-19.

Khiati, A., Sanchez-Moreno, M., Bernard, M., and Joiret, S. 2011. Corrosion inhibition ofcopper in neutral chloride media by a novel derivative of 1,2,4-triazole, *Corrosion Science* **53,** 3092–3099.

Kim, H. C., Kim, M. J., Lim, T., Park, K. J., Kim, K. H., Choe, S., Kim, S. K., Jae Jeong Kim, J. J. 2014. Effects of nitrogen atoms of benzotriazole and its derivatives on the properties of electrodeposited Cu films. *Thin Solid Films* **550,** 421–427.

Kraka, E., and Cremer, D. 2000 Computer design of anticancer drugs. *Journal of American. Chemical Society* **122,** 8245–8264.

Levin, M., Wiklund, P., and Leygraf, C. 2012. Bioorganic compounds as copper corrosion inhibitors in hydrocarbon media. *Corrosion Science* **58,** 104–114.

Li, S., Chen, S., Lei, S., Ma, H., Yu, R., and Liu, D. 1999. Investigation on some Schiff bases as HCl corrosion inhibitors for copper. *Corrosion Science* **41,** 1273 – 1287.

Liao, X., Cao, F., Zheng, L. L. W., Chen, A., Zhang, J., and Cao, C. 2011. Corrosion behaviour of copper under chloride-containing thin electrolyte layer. *Corrosion Science* **53,** 3289-3298.

Lorenz, W.J. and Mansfeld, F. 1981. Determination of corrosion rates by electrochemical DC and AC methods. *Corrosion Science* **21,** 647-672.

Lui, R. 1997. Copper and model fungal secreted ligands. Mater thesis, B.E. Harbin Engineering University.

Melchers, R.E. 2015. Bi-modal trends in the long-term corrosion of copper and high

copper alloys, *Corrosion Science* **95,** 51 – 61.

Moreno-Pirajan, J.C. 2011. *Thermodynamics - Interaction Studies - Solids, Liquids and Gases*, 1st Edition. InTect, Shanghai

Mostafa, H.A., Zaghloul, E.I., and Moussa, M.N. 2002. Corrosion Inhibition of Copper by Some Thiourea Derivatives. *Portuguese Electrochimica Acta* **20,** 83-75.

Muralidharan, S., Phani, K.L.N., Pitchumuni, S., Ravichandran, S., and Iyer, S.V.K. 1995. Polu amino Benzoquinone Polymers: A New Class of Corrosion Inhibitor for Mild Steel. *Journal of the Elelctrochemical Society* **5,** 1478-1483.

Musa, A.Y., Kadhum, A.A.H., Mohamad, A.B., Takriff, M.S., Daud, A.R., and Kamarudin, S.K. 2010. Adsorption isotherm mechanism of amino organic compounds as mild steel corrosion inhibitors by electrochemical measurement method. *Journal of Central South University of Technology* **17,** 34-39.

Musa, A.Y., Jalgham, R.T.T., and Mohamad, A.B. 2012. Molecular dynamic and quantum chemical calculations for phthalhydrazine derivatives as corrosion inhibitors of mild steel in 1 M HCl. *Corrosion Science* **56,** 176-183.

Muthukumar, N., Ilangovan, A., Maruthamuthu, S., Palaniswamy, N., Kimura, A. 2009. 1-Aminoanthraquinone derivatives as a novel corrosion inhibitor for carbon steel API 5L-X60 in white petrol–water mixtures. *Materials Chemistry and Physics* **115,** 444 – 452.

Naqvi, I., Saleemi, A.R., and Naveed, S. 2011. Cefixime: A drug as efficient corrosion inhibitor for mild steel in acidic media. Electrochemical and thermodynamic studies. *International Journal of Electrochemical Science* **6,** 146-161.

Nathan, C.C. 1973 Corrosion Inhibitors, *National Association of Corrosion Engineering*, Houston, Texas, USA

Nicholson, R.S. and Shain, I. 1964. Theory of Stationary Electrode Polarograghy: Single Scan and Cyclic Methods Applied to Reversible, Irreversible, and Kinetics Systems. *Analytical Chemistry* **36,** 706-723.

Nwabanne, J., and Okafor, V. 2012. Adsorption and Thermodynamics Study of the Inhibition of Corrosion of Mild Steel in H_2SO_4 Medium using Vernonia Amygdalina. *Journal of Minerals and Materials Characterization and Engineering* **11,** 885-890.

Pan, Y.C., Wen, Y., Guo, X.Y,, Song, P., Shen, S., Du, Y.P., and Yang, H.F. 2013. 2-Amino-5-(4-pyridinyl)-1,3,4-thiadiazole monolayers on copper surface:Observation of the relationship between its corrosion inhibition and adsorption structure. *Corrosion Science* **73,** 274-280.

Parakala, S.P. 2005. EIS investigation of carbon dioxide and hydrogen sulfide corrosion under film forming. PhD Thesis, Ohio University.

Piccin, J.S., Dotto, G.L., and Pinto. L.L.A. 2011. Adsorption isotherms and thermochemical data of FD&C red N^o 40 binding by chitosan. *Brazilian Journal of Chemical Engineering* **28,** 295-304.

Puerto, E.D., Cuesta, A., Sanchez-Cortez, S., Garcia-Ramos, J.V., and Domingo, C. 2013. Electrochemical SERS study on a copper electrode of the insoluble organic pigment quiacridone quinone using ionic liquids (BMIMCl and TBAN) as dispersing agent. *Analyst* **138,** 4670-4676.

Raafat, M.I., Mohamed, K.A., and Faten, M.A. 2008. Quantum chemical studies on the inhibition of corrosion of copper surface by substituted uracils. *Applied Surface Science* **255,** 2433-2441.

Rajkumar, G., and Sethuraman, M. G. 2014. Corrosion protection ability of self-

assembled monolayer of 3-amino-5-mercapto 1,2,4-triazole on copper electrode. *Thin Solid Films* **562,** 32–36.

Roberge, P.R. 2008. *Corrosion Engineering: Principles and Practice*, McGraw-Hill, New York.

Sayak, R., Biprajit, S., Denis, B., Mark, N., Stanislav, Z.I., Goutam, K.L., and Wolfgang, K. 2008. Stabilizing the Elusive ortho-Quinone/Copper(I) Oxidation State Combination through π/π Interaction in an Isolated Complex. *Journal of the American Chemical Society* **130,** 15230–15231.

Sharif, E-SM., Eramus, R.M., and Comins, J.D. 2007. Effects of 3-amino-1,2,4-triazole on the inhibition of copper corrosion in acidic chloride solutions. *Journal of Colloid and Surface Science* **311,** 144-151.

Shreir, L.L., Jarman, R.A. and G.T. Burstein, G.T. 1994. *Corrosion Control*. 3rd Edition. Butterworths Heinemann, Oxford, U.K.

Soomro, G.A. 2009. Spectrophotometric Determination of Metals with Suitable Chelating Agents in Micellar Media PhD Thesis, Shah Abdul Latif University, Khairpurmir's Sindh, Pakistan.

Souza, F.S.D., Giacomelli, C., Gonçalves, R. S., and Spinelli, A. 2012. Adsorption behavior of caffeine as a green corrosion inhibitor for copper. *Materials Science and Engineering C* 32, 2436–2444.

Stoyanova, A., and Slavcheva, E. 2011. Effect of the molecular structure of some quinones on their corrosion inhibiting action. *Material and Corrosion* **62,** 872 – 877.

Sudheer, and Quraishi, M.A. 2013. Electrochemical and theoretical investigation of triazole derivatives on corrosion inhibition behavior of copper in hydrochloric acid medium. *Corrosion Science* 70, 161–169.

Sun, S., Geng, Y., Tian, L., Chen, S., Yan, Y., and Hu, S. 2012. Density functional theory study of imidazole, benzimidazole and 2-mercaptobenzimidazole adsorption onto clean Cu(111) surface. *Corrosion Science* **63,** 140 –147.

Tansug, G., Tuken, T., Giray, E.S., Findikkiran, G., Sigircik, G., Demirkol, O., Erbil, M. 2014. A new corrosion inhibitor for copper protection. *Corrosion Science* **84,** 21-29.

Taylor, I.F., Weininger, M.S., and Amma, E.L. 1974. Preparation, crystal structure, and bonding in the dimers of tris(thiourea) coppers(I) tetrafluoroborate and tris(s-dimethylthiourea) copper(I) tetrafluoroborate. *Inorganic Chemistry* **13,** 2835–2842.

Thirunarayanan, G., Thirumurthy, K., and Subramania, A. 2011. Influence of Polythiophene-Anthraquinone Sulphonic Acid on the Corrosion Inhibition of Mild Steel in 1N HCl Medium. *The IUP Journal of Chemistry* **5,** 29-40.

Tian, H., Li, W., Cao, K., and Hou, B. 2013. Potent inhibition of copper corrosion in neutral chloride media by novel non-toxic thiadiazole derivatives. *Corrosion Science* **73,** 281-291.

Tian, H., Cheng, Y.F., Li, W., and Hou, B. 2015. Triazolyl-acylhydrazone derivatives as novel inhibitors for copper corrosion in chloride solutions. **100,** 341–352.

Umoren, S.A., and Solomon, M.M. 2015. Effect of halide ions on the corrosion inhibition efficiency of different organic species – A review. *Journal of Industrial and Engineering Chemistry* **21,** 81–100.

Ursula, C. 2013. An electrochemical investigation into the corrosion protection properties of coatings for the active metal copper. PhD Thesis, University of Ireland.

US Patent 3551349 A.

Wang, C.H., Chung, S.Y., Jao, H.J, and Hung, W.H. 2011. Surface-Confined Pyrroloquinoline Quinone: Characterizations and Interactions with Copper Ions, *The Journal of Physical Chemistry* **115,** 1978-1984.

Wang, J. 2000. *Analytical Electrochemistry*. Wiley-VCH. p. *29,* New York.

Wang, Y.H., and He,J. B. 2012. Corrosion inhibition of copper by sodium phytate in NaOH solution: Cyclic voltabsorptometry for in situ monitoring of soluble corrosion products. *Electrochimica Acta* **66,** 45 – 51.

Yadav, S., Choudhary, G., and Sharma. A.l. 2013. Green Approach to Corrosion Inhibition of aluminium and copper by Ziziphus mauritiana Fruit Extract in Hydrochloric Acid Solution. *International Journal of ChemTech Research* **5,** 1815-1823.

Yaro, A., Khadom, A., and Wael, R. 2013 Apricot juice as green corrosion inhibitor of mild steel in phosphoric acid. *Alexandria Engineering Journal* **52,** 129-135.

Yurt, A., Balaban, A., Ustun, K. S., Bereket, G., and Erk, B. 2004. Investigation on some Schiff bass as HCl corrosion inhibitors for carbon steel. *Material Chemistry and Physics* **85,** 420-426.

Zhang, D.Q., Cai, Q. R., He, X.M., Gao, L.X., and Zhou, G.D. 2008. Inhibition effect of some amino acids on copper corrosion in HCl solution. *Materials Chemistry and Physics* **112,** 353–358.

Zhang, J., Qiao, G., Hu, S., Yan, Y., Ren, Z., and Yu, L. 2011. Theoretical evaluation of corrosion inhibition performance of imidazoline compounds with different hydrophilic groups. *Corrosion Science* **53,**147-152.

Zhao, J., and Cui, G. 2011. Study on Adsorption and Complexation Behavior of Thiourea on Copper Surface. *International Journal of Electrochemical Science* **6,** 4048-4058.

Zhang, Q.B., and Hua, Y.X. 2009. Corrosion inhibition of mild steel by alkylimidazolium ionic liquids in hydrochloric acid. *Electrochimica Acta* **54,** 1881-1887.

APPENDICES

APPENDICE A

CORROSION INHIBITION OF COPPER BY THIOUREA AND N, O, S-LIGATING RING COMPOUNDS

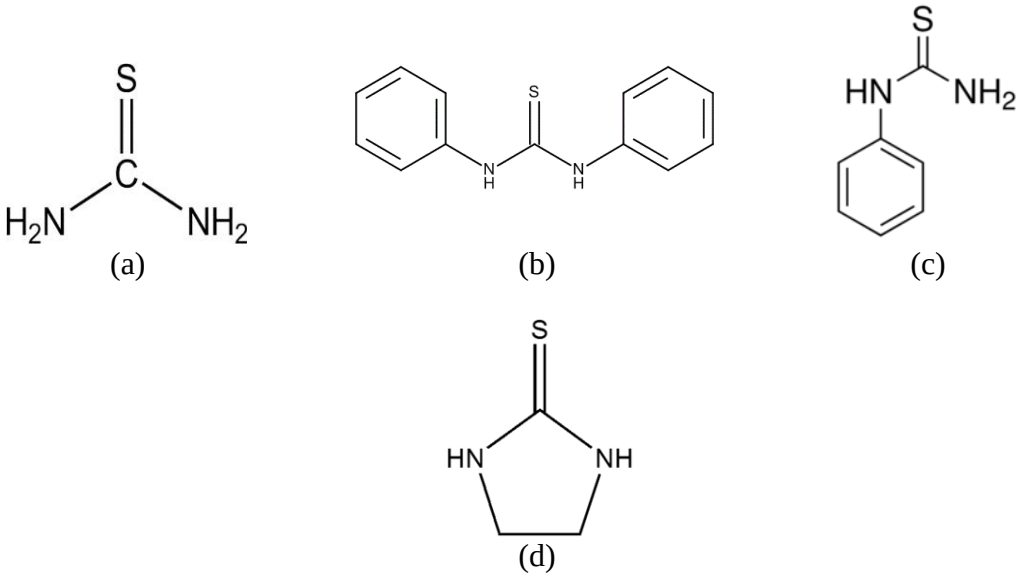

(a) (b) (c)

(d)

Appendix A-1. Structures of thiourea compounds under investigation. Thiourea (a), Diphenylthiourea (b), Phenylthiourea (c), Ethylenethiourea (d)

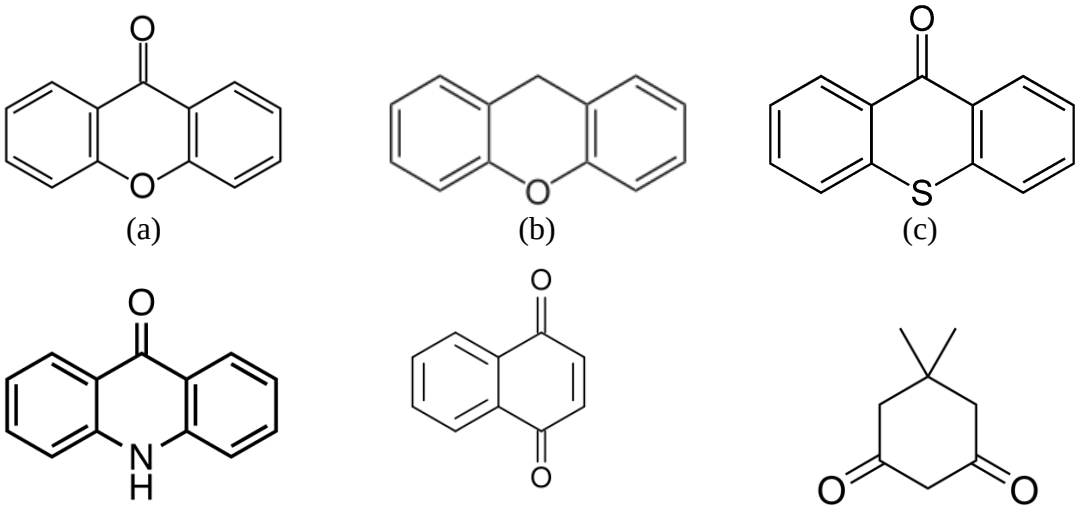

(a) (b) (c)

(d) (e) (f)

Appendix A-2 Structures of quinone derivatives under investigation. Xanthone (a), Xanthene (b), Thioxanthone (c), Acridone (d), 1,4-naphthoquinone (e), Dimedone (f)

Appendix A-3 j_{corr} values for copper in acetonitrile solution in the presence of thioureas at room temperature

Thiourea type (1mM)	j_{corr} (Acm^{-2})			Average	SD	%RSD
	I	II	III			
tu	3.15×10^{-8}	2.95×10^{-8}	2.83×10^{-8}	2.97×10^{-8}	0.16	5.57
dptu	3.99×10^{-8}	3.71×10^{-8}	3.98×10^{-8}	3.89×10^{-8}	0.20	4.16
ptu	3.30×10^{-8}	3.28×10^{-8}	3.18×10^{-8}	3.26×10^{-8}	0.06	2.00
etu	1.93×10^{-8}	2.09×10^{-8}	1.87×10^{-8}	1.96×10^{-8}	0.10	5.66
tu + 1 mM Cl^-	1.07×10^{-5}	1.09×10^{-5}	1.12×10^{-5}	1.10×10^{-5}	0.03	2.36
tu + 1 mM I^-	4.72×10^{-5}	4.66×10^{-5}	4.65×10^{-5}	4.67×10^{-5}	0.04	0.80
tu + 1 mM Br^-	2.33×10^{-5}	2.34×10^{-5}	2.29×10^{-5}	2.32×10^{-5}	0.02	1.19
dptu + 1 mM Cl^-	2.68×10^{-6}	2.62×10^{-6}	2.67×10^{-6}	2.66×10^{-6}	0.03	1.23
dptu + 1 mM I^-	3.88×10^{-5}	4.10×10^{-5}	3.85×10^{-5}	3.95×10^{-5}	0.10	3.43
dptu +1 mM Br^-	2.30×10^{-5}	2.40×10^{-5}	2.49×10^{-5}	2.40×10^{-5}	0.09	3.96
ptu + 1 mM Cl^-	1.02×10^{-5}	1.01×10^{-5}	1.04×10^{-5}	1.02×10^{-5}	0.02	1.75
ptu + 1 mM I^-	4.54×10^{-5}	4.74×10^{-5}	4.66×10^{-5}	4.65×10^{-5}	0.04	2.14
ptu +1 mM Br^-	3.88×10^{-5}	4.06×10^{-5}	3.95×10^{-5}	3.96×10^{-5}	0.09	2.31
etu + 1 mM Cl^-	1.08×10^{-5}	1.04×10^{-5}	1.06×10^{-5}	1.06×10^{-5}	0.02	1.63
etu + 1 mM I^-	4.56×10^{-5}	4.75×10^{-5}	4.63×10^{-5}	4.65×10^{-5}	0.09	2.07
etu+ 1 mM Br^-	1.29×10^{-5}	1.28×10^{-5}	1.23×10^{-5}	1.26×10^{-5}	0.03	2.27
-	3.82×10^{-6}	3.79×10^{-6}	3.82×10^{-6}	3.81×10^{-6}	0.073	0.45

Appendix A-4 j_{corr} values for copper in acetonitrile solution in the presence of N, O, S-ligating ring compounds at room temperature

Ligating ring compounds type (1 mM)	j_{corr} (Acm^{-2})			Average	SD	%RSD
	I	II	III			
Xanthone	9.05×10^{-8}	8.88×10^{-8}	9.19×10^{-8}	9.04×10^{-8}	0.15	1.72
Xanthene	8.42×10^{-8}	8.79×10^{-8}	8.71×10^{-8}	8.64×10^{-8}	0.19	2.24
Thioxanthone	1.13×10^{-7}	1.15×10^{-7}	1.15×10^{-7}	1.14×10^{-7}	0.01	1.00
Acridone	3.86×10^{-8}	3.87×10^{-8}	3.89×10^{-8}	3.87×10^{-8}	0.01	0.34
1,4-napthoquinone	2.72×10^{-7}	2.74×10^{-7}	2.71×10^{-7}	2.74×10^{-7}	0.01	0.43
1,4-napthoquinone + 0.1 M aniline	5.78×10^{-7}	5.62×10^{-7}	5.94×10^{-7}	5.78×10^{-7}	0.02	2.82
1,4-napthoquinone + 0.1 M acetic acid	2.21×10^{-6}	2.22×10^{-6}	2.23×10^{-6}	2.22×10^{-6}	0.01	0.53

APPENDICE B

CORROSION INHIBITION OF COPPER BY DIMEDONE

Appendix B-1 j_{corr} values for copper in acetonitrile solution in the absence and presence of dimedone at different concentrations at room temperature

$C_{dimedone}$ (mM)	j_{corr} (A cm^{-2})			Average	SD	%RSD
	I	II	III			
0.00	3.82×10^{-6}	3.79×10^{-6}	3.82×10^{-6}	3.81×10^{-6}	0.017	0.45
0.25	2.46×10^{-6}	2.49×10^{-6}	2.46×10^{-6}	2.47×10^{-6}	0.017	0.70
0.50	2.41×10^{-6}	2.46×10^{-6}	2.45×10^{-6}	2.44×10^{-6}	0.026	1.08
1.00	1.59×10^{-6}	1.54×10^{-6}	1.55×10^{-6}	1.56×10^{-6}	0.026	1.70
2.00	0.52×10^{-6}	0.51×10^{-6}	0.51×10^{-6}	0.51×10^{-6}	0.002	0.30
3.00	0.44×10^{-6}	0.45×10^{-6}	0.44×10^{-6}	0.44×10^{-6}	0.003	0.57

Appendix B-2 R_{ct} values for copper in acetonitrile solution in the absence and presence of dimedone at different concentrations at room temperature

$C_{dimedone}$ (mM)	R_{ct} (Ω cm^2)			Average	SD	%RSD
	I	II	III			
0.00	63712.24	63713.18	63711.19	63712.20	0.996	0.0016
0.25	88182.27	88181.32	88180.30	88181.30	0.985	0.0011
0.50	88744.99	88743.81	88745.88	88744.90	1.038	0.0012
1.00	104542.90	104541.56	104542.44	104542.30	0.681	0.0007
2.00	117836.23	117837.47	117837.31	117837.00	0.674	0.0006
3.00	123398.70	123398.60	123399.70	123399.00	0.608	0.0005

Appendix B-3 Langmuir adsorption isotherm by EIS measurement of dimedone on copper surface in acetonitrile at room temperature

$C_{dimedone}$ (mM)	*%IE*	$C_{dimedone}/\theta$ (mM)	θ
0.25	38.41	0.6509	0.3841
0.50	39.29	1.2725	0.3929
1.00	64.08	1.5604	0.6408
2.00	84.95	2.3542	0.8495
3.00	93.68	3.2023	0.9368

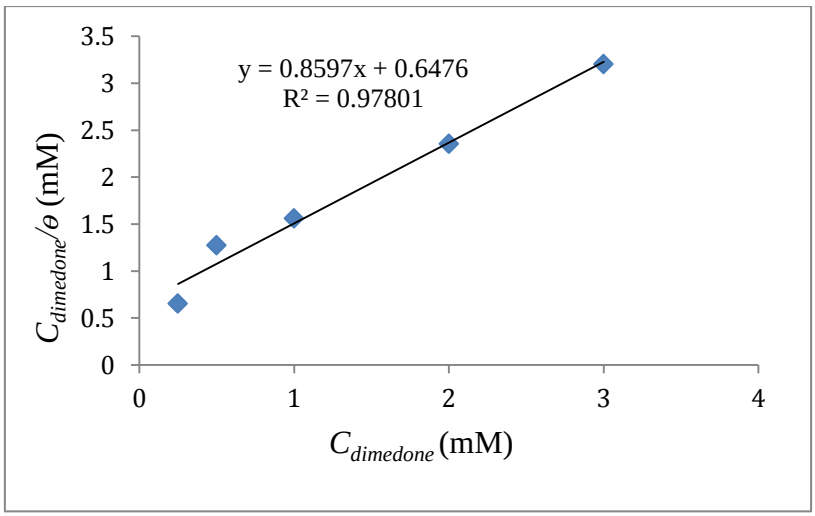

Appendix B-4 Langmuir adsorption isotherm by polarization measurement of dimedone on copper surface in acetonitrile at room temperature

$C_{dimedone}$ (mM)	*%IE*	$C_{dimedone}/\theta$ (mM)	θ
0.25	35.17	0.7108	0.3517
0.50	35.95	1.3908	0.3595
1.00	59.06	1.6932	0.5906
2.00	86.48	2.3127	0.8648
3.00	88.37	3.3948	0.8837

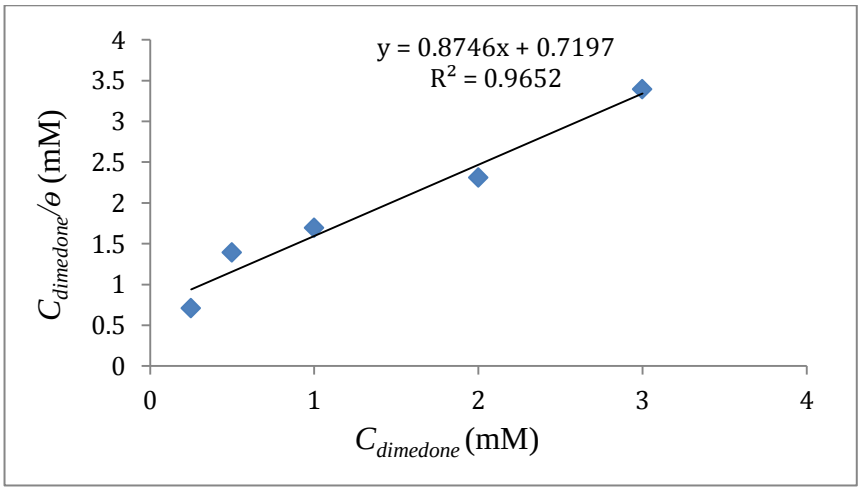

Appendix B-5 Freundlich adsorption isotherm by EIS measurement of dimedone on copper surface in acetonitrile at room temperature

$C_{dimedone}$ (mM)	*%IE*	*ɵ*	*log* $C_{dimedone}$ (mM)	*log ɵ*
0.25	38.41	0.3841	-0.6021	-0.4156
0.50	39.29	0.3929	-0.3010	-0.4057
1.00	64.08	0.6408	0.0000	-0.1932
2.00	84.95	0.8495	0.3010	-0.0708
3.00	93.68	0.9368	0.4771	-0.0283

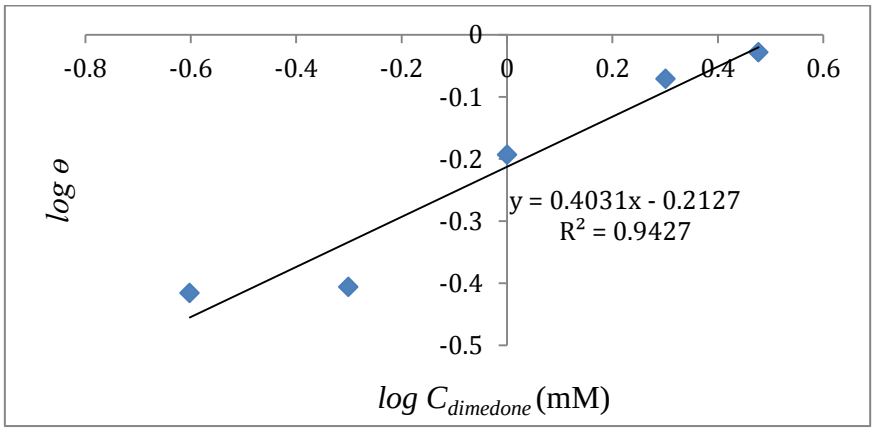

Appendix B-6 Freundlich adsorption isotherm by polarization measurement of dimedone on copper surface in acetonitrile at room temperature

$C_{dimedone}$ (mM)	*%IE*	*ɵ*	*log* $C_{dimedone}$ (mM)	*log ɵ*
0.25	35.17	0.3517	-0.6021	-0.4538
0.50	35.95	0.3595	-0.3010	-0.4443
1.00	59.06	0.5906	0.0000	-0.2287
2.00	86.48	0.8648	0.3010	-0.0631
3.00	88.37	0.8837	0.4771	-0.0537

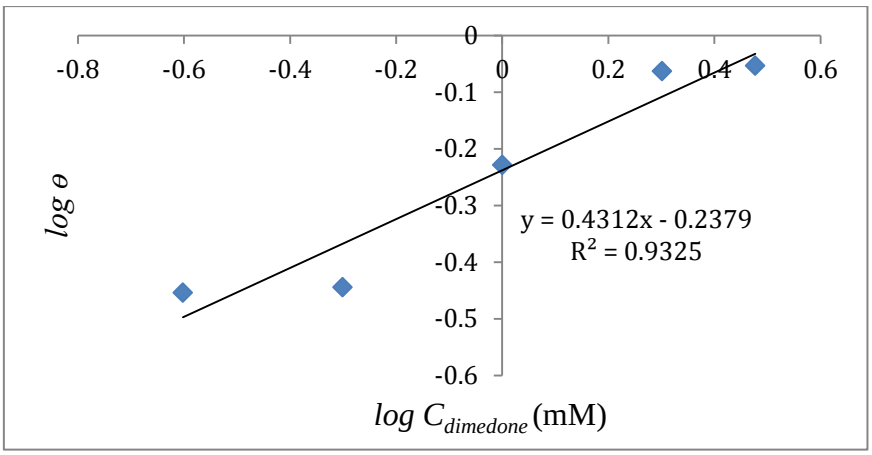

Appendix B-7 Temkin adsorption isotherm by EIS measurement of dimedone on copper surface in acetonitrile at room temperature

$C_{dimedone}$ (mM)	*%IE*	$log\ C_{dimedone}$ (mM)	θ
0.25	38.41	-0.6021	0.3841
0.50	39.29	-0.3010	0.3929
1.00	64.08	0.0000	0.6408
2.00	84.95	0.3010	0.8495
3.00	93.68	0.4771	0.9368

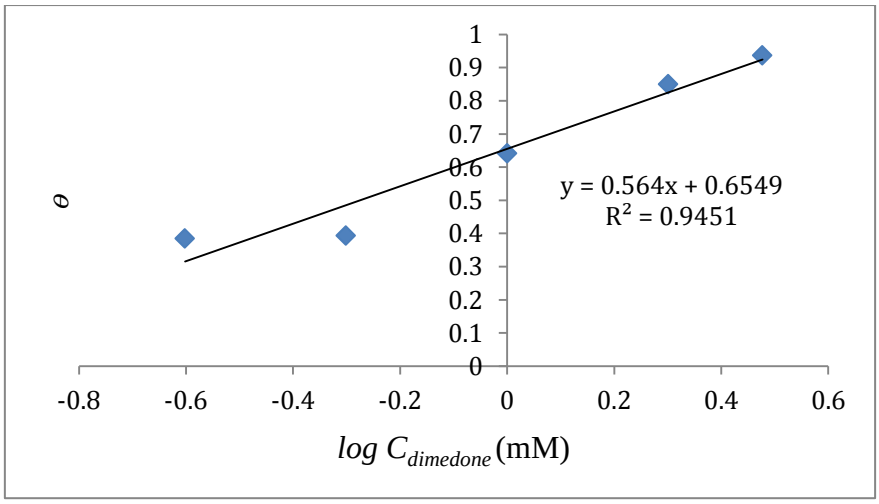

Appendix B-8 Temkin adsorption isotherm by polarization measurement of dimedone on copper surface in acetonitrile at room temperature

$C_{dimedone}$ (mM)	*%IE*	*log* $C_{dimedone}$ (mM)	*θ*
0.25	35.17	-0.6021	0.3517
0.50	35.95	-0.3010	0.3595
1.00	59.06	0.0000	0.5906
2.00	86.48	0.3010	0.8648
3.00	88.37	0.4771	0.8837

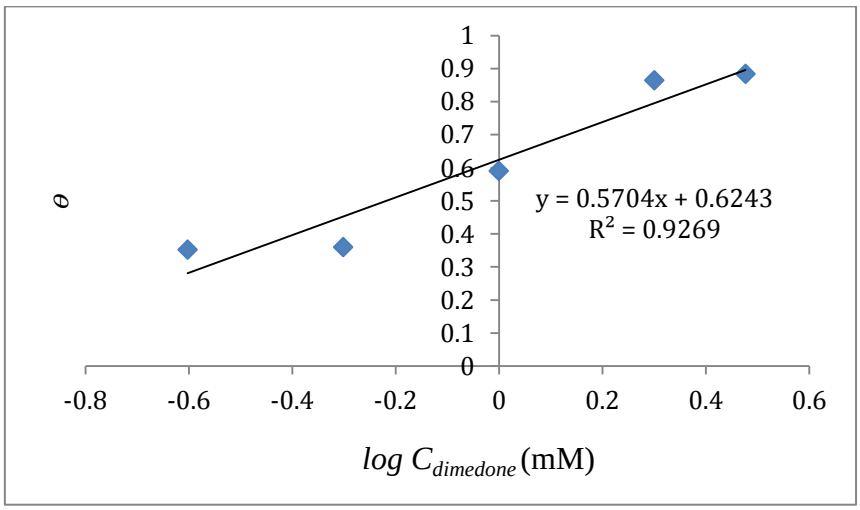

Appendix B-9 Mole ratio of $CuCl_2 \cdot 2H_2O$ with dimedone (λmax = 246 nm) in acetonitrile solution

Ratio between [Cu(II)]/[Dimedone]	**Absorbance**			**Average**	**SD**	**%RSD**
1 : 0.8	0.6468	0.6470	0.6448	0.6462	0.0012	0.1883
1 : 0.9	0.6364	0.6375	0.6377	0.6372	0.0007	0.1099
1 : 1.0	0.6539	0.6542	0.6512	0.6531	0.0017	0.2530
1 : 2.0	0.6746	0.6756	0.6772	0.6758	0.0013	0.1941
1 : 3.0	0.6755	0.6773	0.6770	0.6766	0.0010	0.1425
1 : 4.0	0.6751	0.6754	0.6681	0.6729	0.0041	0.6319

APPENDICE C

CALCULATION OF *IE%*

Appendix C-1 Calculation of *IE%* from the corrosion current density (*j*) in the case of 1 mM of thiourea in acetonitrile

$$IE(\%) = \frac{j_{corr} - j_{inh}}{j_{corr}} \times 100$$

$$IE(\%) = \frac{3.81 \times 10^{-6} - 2.97 \times 10^{-8}}{3.81 \times 10^{-6}} \times 100$$

$$IE(\%) = 99.22$$

Appendix C-2 Calculation of *IE%* from the charge transfer resistance (R_{ct}) in the case of 1 mM of dimedone in acetonitrile

$$IE\% = \frac{R_{ct} - R_{ct}^{0}}{R_{ct}^{0}} \times 100$$

$$IE\% = \frac{104542.30 - 63712.20}{63712.20} \times 100$$

$$IE\% = 64.09$$

APPENDICE D

STATISTICAL ANALYSIS

Appendix D-1 The compared of IE% values of potentiodynamic polarization and EIS measurements for dimedone in acetonitrile solution

t-Test: Paired Two Sample for Means

	Variable 1	*Variable 2*
Mean	48.40333	50.83833
Variance	1223.262	1159.649
Observations	6	6
Pearson Correlation	0.946612	
Hypothesized Mean Difference	0	
df	5	
t Stat	-0.52715	
P(T<=t) one-tail	0.310318	
t Critical one-tail	2.015048	
P(T<=t) two-tail	0.620636	
t Critical two-tail	2.570582	

VITAE

Name Mr. Sontaya Manaboot

Student ID 5610220135

Educational Attainment

Degree	Name of Institution	Year of Graduation
Bachelor of Science (Chemistry)	Songkhla Rajabhat University	2013

Scholarship Awards during Enrolment

Faculty of Science and Graduate School, Prince of Songkla University.

List of Publication and Proceeding

Manaboot, S., Chooto, P., and Weena Aemaeg Tapachai, W.A., "Corrosion inhibition of copper by thioureas and N, O, S-ligating ring compounds" Pure and Applied Chemistry International Conference (PACCON 2016), 9^{th} – 11^{th}, February, 2016, Bangkok International Trade and Exhibition Centre (BITEC), Bangkok, Thailand.